Dear Editor Folberth,

Please find below our itemized responses to the reviewers' comments and a marked-up manuscript. We have addressed all the comments raised by both reviewers and incorporated them in the revised manuscript.

Thank you for your consideration.

Sincerely,
Lin Zhang, Tongwen Wu, Xiao Lu et al.

Reviewer #1

Comment#1-1: This paper describes a framework and evaluation of a novel model framework which incorporates the GEOS-Chem 1-D atmospheric chemistry component into the Beijing Climate Center's Atmospheric GCM (BCC-AGCM). With this combination successfully established, the authors evaluate the model in comparison with a suite of observations, including for tropospheric ozone, OH concentrations, and methane chemical lifetimes. They also compare satellite observations of various important atmospheric measurements, including NO2, CO, SO2, CH2O, and AOD. The work is a significant step forward in the development of Earth System Models in China and is clearly relevant to readers of GMD, and should be accepted pending the authors addressing a few relatively minor points relating to the reproducibility and presentation quality of their manuscript.
Response#1-1: We thank the reviewer for the valuable comments. All of them have been implemented in the revised manuscript. Please see our itemized responses below.

Comment#1-2: Specific Comments: Table 3: it is not clear how oceanic trace gas emissions are parameterized in this work. The work does reference the use of CMIP5 DMS emissions from the ocean in line 204, but Table 3 shows that an oceanic emission of acetone was also included. While this inclusion makes sense given recent research on the subject, it is not clear how this source was decided upon or how it was represented. The representation of the oceanic source of NH3 listed in Table 3 is also unexplained. Additionally, the ocean is a known source of acetaldehyde (Millet et al., 2010; Wang et al., 2019), but this source is not accounted for in Table 3. It is not discussed in the paper why this is the case.

References:
Millet, D. B., Guenther, A., Siegel, D. A., Nelson, N. B., Singh, H. B., de Gouw, J. A., et al. (2010). Global atmospheric budget of acetaldehyde: 3-D model analysis and constraints from in-situ and satellite observations. Atmospheric Chemistry and Physics, 10(7), 3405–3425. https://doi.org/10.5194/acp-10-3405-2010

Wang, S., Hornbrook, R. S., Hills, A., Emmons, L. K., Tilmes, S., Lamarque, J. F., et al. (2019). Atmospheric Acetaldehyde: Importance of Air-Sea Exchange and a Missing Source in the Remote Troposphere. Geophysical Research Letters, 46(10), 5601–5613. https://doi.org/10.1029/2019GL082034

Response#1-2: Thanks for pointing it out. The oceanic emissions of acetone and ammonia (NH3) are obtained from the Atmospheric Chemistry and Climate Model Intercomparison Project (ACCMIP) emission inventory (Lamarque et al., 2010). We indeed did not consider the oceanic acetaldehyde emissions, which should be addressed in the next model version.

We now state in the Section 2.5.1 (Offline emissions): "We also incorporate emissions from the Atmospheric Chemistry and Climate Model Intercomparison Project (ACCMIP) inventory (http://accent.aero.jussieu.fr/ACCMIP.php, last access: 14 Jun 2020; Lamarque et al., 2010) and from Wu et al. (2020) for emissions not included in CEDS data set. These mainly apply to oceanic emissions, soil NO_x emissions, and volcanic SO_2 emissions. Several sources (e.g., oceanic acetaldehyde emissions (Millet et al., 2010; Wang et al., 2019)) have not yet been included in this model version."

Reference added:

Lamarque, J. F., Bond, T. C., Eyring, V., Granier, C., Heil, A., Klimont, Z., Lee, D., Liousse, C., Mieville, A., Owen, B., Schultz, M. G., Shindell, D., Smith, S. J., Stehfest, E., Van Aardenne, J., Cooper, O. R., Kainuma, M., Mahowald, N., McConnell, J. R., Naik, V., Riahi, K., and van Vuuren, D. P.: Historical (1850–2000) gridded anthropogenic and biomass burning emissions of reactive gases and aerosols: methodology and application, Atmos. Chem. Phys., 10, 7017-7039, http://doi.org/10.5194/acp-10-7017-2010, 2010.

Millet, D. B., Guenther, A., Siegel, D. A., Nelson, N. B., Singh, H. B., de Gouw, J. A., Warneke, C., Williams, J., Eerdekens, G., Sinha, V., Karl, T., Flocke, F., Apel, E., Riemer, D. D., Palmer, P. I., and Barkley, M.: Global atmospheric budget of acetaldehyde: 3-D model analysis and constraints from in-situ and satellite observations, Atmos. Chem. Phys., 10, 3405-3425, http://doi.org/10.5194/acp-10-3405-2010, 2010.

Wang, S., Hornbrook, R. S., Hills, A., Emmons, L. K., Tilmes, S., Lamarque, J. F., Jimenez, J. L., Campuzano-Jost, P., Nault, B. A., Crounse, J. D., Wennberg, P. O., Kim, M., Allen, H., Ryerson, T. B., Thompson, C. R., Peischl, J., Moore, F., Nance, D., Hall, B., Elkins, J., Tanner, D., Huey, L. G., Hall, S. R., Ullmann, K., Orlando, J. J., Tyndall, G. S., Flocke, F. M., Ray, E., Hanisco, T. F., Wolfe, G. M., St. Clair, J., Commane, R., Daube, B., Barletta, B., Blake, D. R., Weinzierl, B., Dollner, M., Conley, A., Vitt, F., Wofsy, S. C., Riemer, D. D., and Apel, E. C.: Atmospheric Acetaldehyde: Importance of Air-Sea Exchange and a Missing Source in the Remote Troposphere, Geophys. Res. Lett., 46, 5601-5613, http://doi.org/10.1029/2019gl082034, 2019.

Wu, T., Zhang, F., Zhang, J., Jie, W., Zhang, Y., Wu, F., Li, L., Yan, J., Liu, X., Lu, X., Tan, H., Zhang, L., Wang, J., and Hu, A.: Beijing Climate Center Earth System Model version 1 (BCC-ESM1): model description and evaluation of aerosol simulations, Geoscientific Model Development, 13, 977-1005, http://doi.org/10.5194/gmd-13-977-2020, 2020.

Comment#1-3: Figure 6: The y-Axis is unlabeled and not clearly explained in the caption. I assume this is ozone in ppb, but some label or caption edit is probably in order. More importantly, it is not clear from the discussion of Figure 6 and Figure 3 whether the simulated values are taken from GEOS-Chem over some defined region or simply from the grid boxes corresponding to the observations in Figure 3.

Response#1-3: We have added the label "Ozone mixing ratio [ppbv]" for the y-axis in Figure 6. We now also state in Section 3.1 (Observations used for model evaluation): "<u>To derive the monthly mean ozone profiles, only sites and months with more than three observations per month are considered, and simulated monthly mean ozone profiles are sampled over the corresponding model grids (Lu et al., 2019b).</u>"

Reference added:

Lu, X., Zhang, L., Zhao, Y., Jacob, D. J., Hu, Y., Hu, L., Gao, M., Liu, X., Petropavlovskikh, I., McClure-Begley, A., and Querel, R.: Surface and tropospheric ozone trends in the Southern Hemisphere since 1990: possible linkages to poleward expansion of the Hadley circulation, Science Bulletin, 64, 400-409, http://doi.org/10.1016/j.scib.2018.12.021, 2019b.

Comment#1-4: I have questions about the choices of regions used in Figures 3 and 6, though I recognize the authors are referencing regions already in the literature. In particular, I do not agree with the classification of the "NH Low Latitude" grouping in the context of this paper: lumping together southern China, Hawaii, Panama, French Guiana, and Nigeria into one coherent region would to elide an enormous amount of difference in chemical regimes, biomass burning, and anthropogenic emissions between the various regions chosen. I believe it makes more sense to separate the points near China and Taiwan into a "Southeast Asia" region, separate from the remaining "NH Low Latitude" grouping. As the "SH midlatitude" region already has an N of 2, this should be similarly acceptable. This choice may have ramifications for the seasonal simulation performance as summarized in Figure 6.

Response#1-4: Thanks for pointing it out. We have followed the reviewer's suggestion and separated the original "NH Low Latitude" group into the "Southeast Asia" and "NH Low Latitude" groups. Figures 3, 5, and 6 are re-plotted and they do not affect our analysis.

Comment#1-5: Figure 7: The choice made to show observations as small circles on a global map is very confusing in this context. Given the density of spatial coverage over the Northeastern US and Europe, I suggest 3 possible fixes. 1) grid the observations to the same resolution as the model output and show them side-by-side with the simulated ozone; 2) show different plots for the US, for Europe, and for the rest of the globe if necessary; or 3) the points should be averaged for display purposes over a larger spatial extents and made larger themselves. The currently displayed global view could be placed in the SI. As of now, Figure 7 serves a mostly pro forma purpose – it is hard for me to glean any useful information from the plot given the display, and true patterns in the observation data (for example the increase in surface ozone in the observations over central Europe) are obscured by the chosen plotting scheme, rather than illustrated. If the authors do not believe that Figure 7 should be changed, perhaps it belongs in the SI in its entirety, as it is not clear to me what the figure adds to the paper in its current state.

Response#1-5: We agree. We have revised Figure 7 as attached below to show a side-by-side comparison of simulated and observed surface ozone at the same model grids. This change does not affect our analysis.

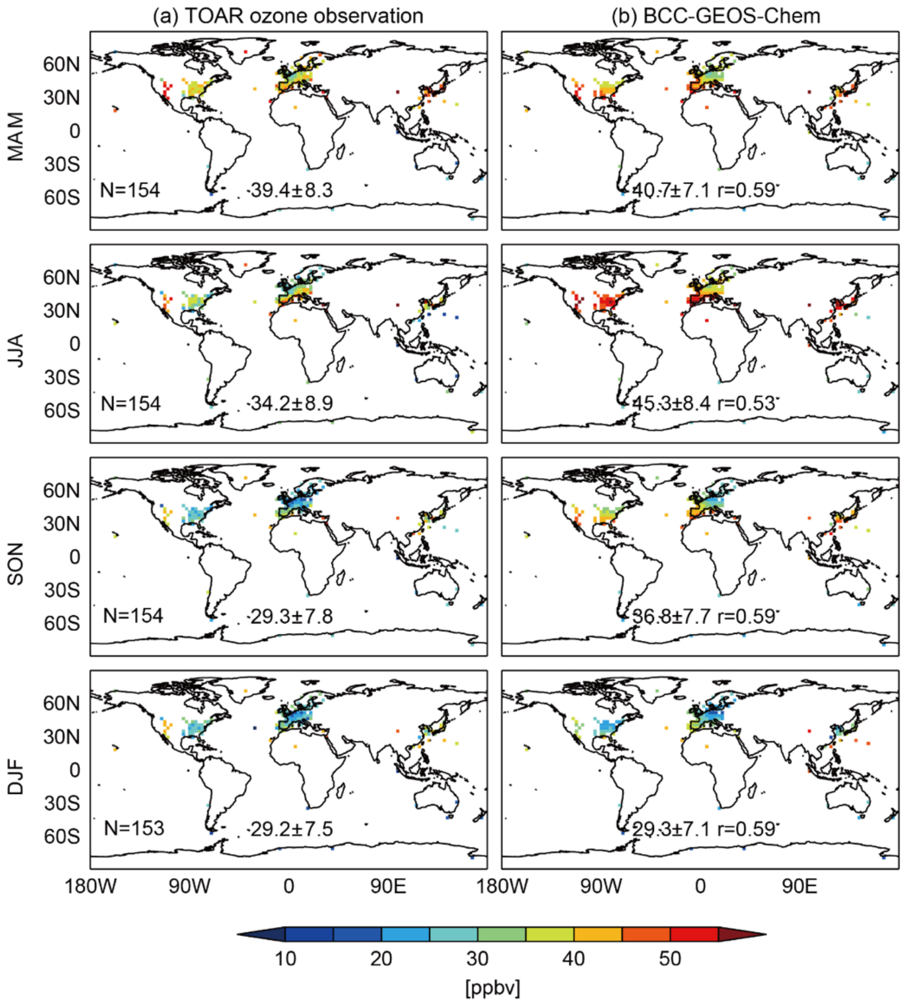

Figure 7. Spatial and seasonal distributions of observed and simulated surface ozone mixing ratios over 2012-2014. The model results (right panels) are compared to observations at rural/remote sites from the TOAR dataset (left panels). Observations are averaged to the same model grid. Seasonal mean values for observations and model results, their spatial correlation coefficients (*r*), and the number of co-sampled grids (N) are shown inset.

Comment#1-6: Figure 8: This is an excellent figure – very clear, with a high information-to-ink ratio. One comment: it seems unlikely that the geographic equator is a meaningful division in this kind of global average, given that the 'meteorological equator' deviates from 0 degrees depending upon season and region. If the comparison datasets support the option, the authors should consider using 5 latitude bins instead of 4 – perhaps 90-50S, 50-20 S, 20 S - 20 N, 20-50 N, and 50-90 N? This has the benefit of treating the tropics, midlatitudes, and polar-latitudes differently.

Response#1-6: Thank you for the nice words on the figure. We agree that using latitude bins of 90-50S, 50-20S, 20S-20N, 20-50N, and 50-90N can be better. However, the results of Young et al. (2013) and Emmons et al. (2010) are presented as the given latitude averages and we followed here to compare with their results.

Reference:

Emmons, L. K., Walters, S., Hess, P. G., Lamarque, J. F., Pfister, G. G., Fillmore, D., Granier, C., Guenther, A., Kinnison, D., Laepple, T., Orlando, J., Tie, X., Tyndall, G., Wiedinmyer, C., Baughcum, S. L., and Kloster, S.: Description and evaluation of the Model for Ozone and Related chemical Tracers, version 4 (MOZART-4), Geoscientific Model Development, 3, 43-67, http://doi.org/10.5194/gmd-3-43-2010, 2010.

Young, P. J., Archibald, A. T., Bowman, K. W., Lamarque, J. F., Naik, V., Stevenson, D. S., Tilmes, S., Voulgarakis, A., Wild, O., Bergmann, D., Cameron-Smith, P., Cionni, I., Collins, W. J., Dalsøren, S. B., Doherty, R. M., Eyring, V., Faluvegi, G., Horowitz, L. W., Josse, B., Lee, Y. H., MacKenzie, I. A., Nagashima, T., Plummer, D. A., Righi, M., Rumbold, S. T., Skeie, R. B., Shindell, D. T., Strode, S. A., Sudo, K., Szopa, S., and Zeng, G.: Pre-industrial to end 21st century projections of tropospheric ozone from the Atmospheric Chemistry and Climate Model Intercomparison Project (ACCMIP), Atmos. Chem. Phys., 13, 2063-2090, http://doi.org/10.5194/acp-13-2063-2013, 2013.

Comment#1-7: Figure 10: why is the discrepancy between modeled and observed SO2 not discussed further? It is true that the model does broadly reproduce the spatial trend observed over China and India but elsewhere the correlation would appear to be quite poor.

Response#1-7: Thanks for pointing it out. We have partly reduced the discrepancies between the observed and modelled SO_2, by removing OMI measurements with slant columns greater than 5 Dobson Units (1.34×10^{17} molecules cm^{-2}) which are affected by strong eruptive volcanoes (Lee et al., 2009, 2011).

We further state in Section 3.4 (Evaluation of other atmospheric constituents) “We find low biases in the modelled PBL SO_2 especially over the volcanic eruption regions (e.g., Central Africa) but high biases in the industrialized regions such as East Asia, a pattern consistent with previous comparisons between the OMI and GEOS-Chem PBL SO_2 columns, which may reflect inappropriate ship and volcanic emissions in the model (Lee et al., 2009) and/or the model bias in the PBL height.”

Reference added:

Lee, C., Martin, R. V., van Donkelaar, A., O'Byrne, G., Krotkov, N., Richter, A., Huey, L. G., and Holloway, J. S.: Retrieval of vertical columns of sulfur dioxide from SCIAMACHY and OMI: Air mass factor algorithm development, validation, and error analysis, J. Geophys. Res., 114, http://doi.org/10.1029/2009jd012123, 2009.

Lee, C., Martin, R. V., van Donkelaar, A., Lee, H., Dickerson, R. R., Hains, J. C., Krotkov, N., Richter, A., Vinnikov, K., and Schwab, J. J.: SO2emissions and lifetimes: Estimates from inverse modeling using in situ and global, space-based (SCIAMACHY and OMI) observations, J. Geophys. Res., 116, http://doi.org/10.1029/2010jd014758, 2011.

Comment#1-8: Technical Corrections: Line 448: Citation is misspelled – should be "Kodros and Pierce, 2017". The reference is correctly spelled in the bibliography.
Response#1-8: Corrected.

Reviewer #2

Comment#2-1: The manuscript presents an overview and assessment of a newly constructed chemistry-climate model that has resulted from the linking of GEOS-Chem with the Beijing Climate Center AGCM. The general features of the model are presented and a fairly extensive comparison against observations for ozone are presented. In addition, other aspects of the model chemical climate are presented, including the global distribution of OH, ozone budget terms, and some limited comparisons for aerosol quantities against observations including AOD and speciated aerosol concentrations over the US.

The manuscript is very clearly written and presented, providing a fairly complete overview of the model components and an idea of how the chemical climate of BCC GEOS-Chem compares with GEOS-Chem itself and with other chemistry climate models.
Response#2-1: We thank the reviewer for the valuable comments. All of them have been implemented in the revised manuscript. Please see our itemized responses below.

Comment#2-2: My only significant criticism is focused on Figure 10, comparing column amounts of NO2, CO, SO2 and CH2O. In the discussion of Figure 10, lines 394 – 404, the authors say that the averaging kernels for the satellite observations were not applied to the model concentrations when calculating the column amounts and that the comparisons 'mainly focus ... on spatial variations rather than absolute magnitudes.' In this case the comparison is nothing more than a test to make sure the specified emissions are being put into the model in the correct locations. Global models have a long-standing low bias for CO in the northern hemisphere that appears to be related to emissions and the hydroxy radical, but Figure 10 shows that BCC-GEOS-Chem has too high CO in the Northern Hemisphere. Due to the lack of a quantitative comparison with the satellite data by application of the averaging kernel it is impossible to judge whether the differences signify anything. While CH2O is not predominantly due to direct emission, the spatial distribution is tightly coupled to the emissions of biogenic hydrocarbons, so the comparison will also be largely driven by having regions of high biogenic emissions in the correct place. The differences in the magnitude of CH2O between the satellite and model is quite large and it would be interesting to have a more quantitative comparison with the satellite observations as the qualitative comparison focused on the spatial distribution is not informative at all. I would strongly urge the authors to revise the comparison of the column amounts to be more quantitative by application of the appropriate averaging kernel. My other comments are all minor in nature and are given below.

Response#2-2: We agree with the reviewer on the need to improve the comparison and discussion for these chemical constituents. For CO, we have now applied the satellite averaging kernels to smooth the model results, and focus on the comparison at 700 hPa where MOPITT has generally high sensitivities. As shown in the new Fig. 10a, the large model high bias has been significantly improved though still exists. For other constituents, however, we do not apply corresponding averaging kernel, which requires additional 3-year model simulation to co-sample observations along the satellite tracks. Previous studies (Zhu et al., 2016; 2020) showed CH_2O shape factor (a prior) was not the main driver of the discrepancy between GEOS-Chem modeled and retrieved columns. Their studies also revealed that satellite CH_2O retrievals showed significant low bias (up to 50%) compared to aircraft measurements, which may largely explain the model high bias as shown here. For SO_2, we have partly reduced the discrepancies between the observed and modelled SO_2, by removing OMI measurements with slant columns greater than 5 Dobson Units (1.34×10^{17} molecules cm^{-2}) which are affected by strong eruptive volcanoes (Lee et al., 2009, 2011).

We have added much more discussions in Section 3.4 (Evaluation of other atmospheric constituents)

"Figure 10 compares the spatial distributions of annual mean simulated CO, NO_2, SO_2, and CH_2O with satellite observations. We evaluate CO at 700 hPa where MOPITT satellite has generally high sensitivity (Emmons et al., 2004; Pfister et al., 2005), and apply averaging kernel to smooth the modelled CO. As shown in Figure 10, BCC-GEOS-Chem v1.0 reproduces the high CO levels over the northern mid-latitudes driven by high anthropogenic sources, and over the central Africa driven by biomass burning emissions (spatial correlation coefficient r=0.92) with some overestimates. It also captures the observed hotspots of tropospheric NO_2 (r=0.87) and PBL SO_2 columns (r=0.32) over East Asia that generally follow the distribution of anthropogenic sources. The sharp land-ocean gradients for both tracers reflect their short chemical lifetime. We find low biases in the modelled PBL SO_2 especially over the volcanic eruption regions (e.g., Central Africa) but high biases in the industrialized regions such as East Asia, a pattern consistent with previous comparisons between the OMI and GEOS-Chem PBL SO2 columns, which may reflect inappropriate ship and volcanic emissions in the model (Lee et al., 2009) and/or the model bias in the PBL height. High levels of tropospheric CH_2O column are simulated over the Amazon, the central Africa, tropical Asia, and the southeastern US, where CH_2O oxidized from large biogenic emissions of VOCs

(*r*=0.67), but the model shows notable overestimates. Previous studies (Zhu et al., 2016; 2020) showed that satellite CH_2O retrievals are biased low by 20–51% compared to aircraft measurements which would partly explain the model bias. Future assessments are required to correct the biases of these gaseous pollutants.”

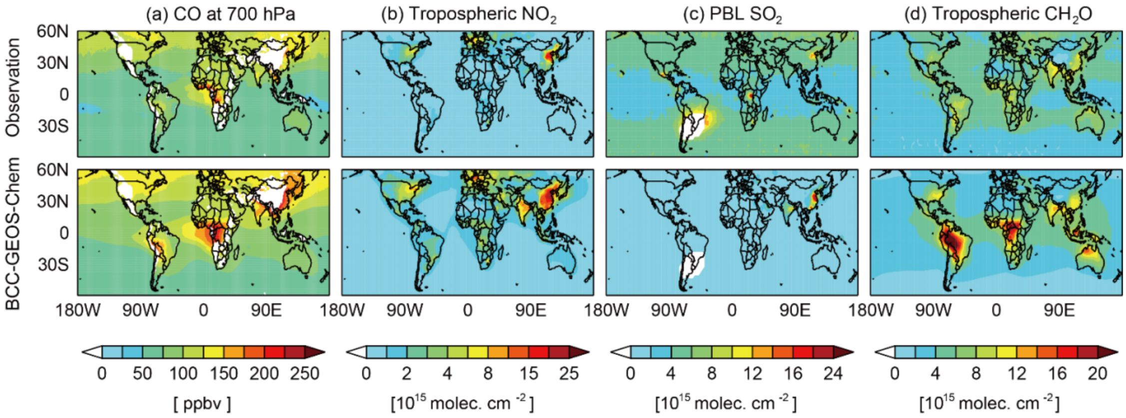

Figure 10. Spatial distributions of satellite observed (top panels) and model simulated (bottom panels) annual mean (a) CO mixing ratio at 700 hPa, (b) tropospheric NO_2 column, (c) SO_2 column in planetary boundary layer, and (d) tropospheric CH_2O column,. Values are 3-year averages for 2012-2014.

References added:

Emmons, L. K., Deeter, M. N., Gille, J. C., Edwards, D. P., Attié, J. L., Warner, J., Ziskin, D., Francis, G., Khattatov, B., Yudin, V., Lamarque, J. F., Ho, S. P., Mao, D., Chen, J. S., Drummond, J., Novelli, P., Sachse, G., Coffey, M. T., Hannigan, J. W., Gerbig, C., Kawakami, S., Kondo, Y., Takegawa, N., Schlager, H., Baehr, J., and Ziereis, H.: Validation of Measurements of Pollution in the Troposphere (MOPITT) CO retrievals with aircraft in situ profiles, J. Geophys. Res., 109, n/a-n/a, http://doi.org/10.1029/2003jd004101, 2004.

Lee, C., Martin, R. V., van Donkelaar, A., O'Byrne, G., Krotkov, N., Richter, A., Huey, L. G., and Holloway, J. S.: Retrieval of vertical columns of sulfur dioxide from SCIAMACHY and OMI: Air mass factor algorithm development, validation, and error analysis, J. Geophys. Res., 114, http://doi.org/10.1029/2009jd012123, 2009.

Lee, C., Martin, R. V., van Donkelaar, A., Lee, H., Dickerson, R. R., Hains, J. C., Krotkov, N., Richter, A., Vinnikov, K., and Schwab, J. J.: SO2emissions and lifetimes: Estimates from inverse modeling using in situ and global, space-based (SCIAMACHY and OMI) observations, J. Geophys. Res., 116, http://doi.org/10.1029/2010jd014758, 2011.

Pfister, G., Hess, P. G., Emmons, L. K., Lamarque, J. F., Wiedinmyer, C., Edwards, D. P., Petron, G., Gille, J. C., and Sachse, G. W.: Quantifying CO emissions from the 2004 Alaskan wildfires using MOPITT CO data, Geophys. Res. Lett., 32, http://doi.org/Artn L1180910.1029/2005gl022995, 2005.

Zhu, L., Jacob, D. J., Kim, P. S., Fisher, J. A., Yu, K., Travis, K. R., Mickley, L. J., Yantosca, R. M., Sulprizio, M. P., De Smedt, I., Abad, G. G., Chance, K., Li, C., Ferrare, R., Fried, A., Hair, J. W., Hanisco, T. F., Richter, D., Scarino, A. J., Walega, J., Weibring, P., and Wolfe, G. M.: Observing atmospheric formaldehyde (HCHO) from space: validation and intercomparison of six retrievals from four satellites (OMI, GOME2A, GOME2B, OMPS) with SEAC(4)RS aircraft observations over the Southeast US, Atmos. Chem. Phys., 16, 13477-13490, http://doi.org/10.5194/acp-16-

13477-2016, 2016.

Zhu, L., González Abad, G., Nowlan, C. R., Chan Miller, C., Chance, K., Apel, E. C., DiGangi, J. P., Fried, A., Hanisco, T. F., Hornbrook, R. S., Hu, L., Kaiser, J., Keutsch, F. N., Permar, W., St. Clair, J. M., and Wolfe, G. M.: Validation of satellite formaldehyde (HCHO) retrievals using observations from 12 aircraft campaigns, Atmospheric Chemistry and Physics Discussions, http://doi.org/10.5194/acp-2019-1117, 2020.

Comment#2-3: Lines 80 - 83: Here the authors state 'Integration of GEOS-Chem chemical module into CSMs has been enabled by separating the module (which simulates all local processes including chemistry, deposition, and emission) from the simulation of transport, and making it operate on 1-D (vertical) columns in a grid-independent manner (Long et al., 2015; Eastham et al., 2018).' How is the 1-D column version of GEOS-Chem integrated with a 3-D CSM for processes that typically occur in the physics of the model such as vertical turbulent diffusion and transport by deep convection? (I do find a description of deep convection and wet deposition around line 190, but no mention of how vertical diffusion is performed.)

Response#2-3: Thanks for pointing it out. The vertical diffusion of the tracers is parameterized using a non-local scheme as described in Holtslag and Boville (1993). We now state in the Section 2.2 (Atmospheric Chemistry): "Tracer advection in BCC-GEOS-Chem v1.0 is performed using a semi-Lagrangian scheme (Williamson and Rasch, 1989) and the vertical diffusion within the boundary layer follows the parameterization of Holtslag and Boville (1993)"

Reference added:

Holtslag, A. A. M. and Boville, B. A.: Local versus nonlocal boundary-layer diffusion in a global climate model, J. Climate, 6, 1825–1842, 1993.

Comment#2-4: Lines 181 – 183: The dry deposition uses the general characteristics of the land surface as given by the CSM land module BCC-AVIM. Are there also links to the land surface scheme for more short-term variables such as stomatal resistance, that would allow for effects such as drought on dry deposition?

Response#2-4: The stomatal conductance is simulated but its influences on dry deposition are not considered, therefore the model does not allow drought influences the dry deposition through modulating stomatal conductance so far. We now state in Section 2.5 (Dry and wet deposition) "Variables needed for the dry deposition calculation such as the friction velocity, Monin-Obukhov length, and leaf area index (LAI) are obtained from the atmospheric dynamics/physics modules or the land module BCC-AVIM, based on which GEOS-Chem calculates the aerodynamic, boundary-layer, and surface resistances. The impacts of some other short-term land variables, such as stomatal conductance, on dry deposition are not included yet."

Comment#2-5: Line 234: Minor typo in 'The model estimates t global annual ...'

Response#2-5: Corrected.

Comment#2-6: Lines 311 – 314: Somewhere, either in the discussion of Figure 5 or the caption, there should be mention that the comparison is for annual average ozone.
Response#2-6: Thanks for pointing it out. We now state "As shown in Figure 5, the model well reproduces the observed annual mean ozone vertical structures…". We have also revised the figure caption accordingly.

Comment#2-7: Lines 314 – 321: I was a bit curious about why the vertical profile of ozone for the Japanese stations shows such a different vertical structure between the observations and model in Figure 5. Looking at Figure 6, the 300 hPa doesn't show that big of a difference. If 300 hPa is somewhere around 10 – 11 km, shouldn't the annual average in the observations be over 120 ppbv, though it is listed as 90 ppbv on Figure 6?
Response#2-7: 300hPa over Japan is around 9 km, and therefore Figures 5 and 6 are consistent. This is a region with frequent stratosphere to troposphere transport and the model may have difficulty in capturing the sharp ozone increases with increasing altitude there.

Comment#2-8: Line 364: Discussing the discrepancy in OH in the tropics between the Spivakovsky climatology the authors state 'This discrepancy appears to be mainly driven by the high bias in ozone levels in this region.' Attempts to understand the reasons for differences in OH between models has shown how many different factors play a role – see, for example, Nicely et al. Atmos. Chem. Phys. 20, doi:10.5194/acp-20-1341-2020, 2020. Do the authors have some reason to believe that the ozone and hydroxyl biases are related and, if not I would suggest removing this statement.
Response#2-8: Thanks for pointing it out. We agree that the OH discrepancies in the model can be driven by more factors than the ozone bias. We now change the statement to "Discrepancies in modeling climate and concentrations of methane, ozone, NOx, and CO can all contribute to the OH bias in climate-chemistry models (Nicely et al., 2020)."

Reference added:

Nicely, J. M., Duncan, B. N., Hanisco, T. F., Wolfe, G. M., Salawitch, R. J., Deushi, M., Haslerud, A. S., Jöckel, P., Josse, B., Kinnison, D. E., Klekociuk, A., Manyin, M. E., Marécal, V., Morgenstern, O., Murray, L. T., Myhre, G., Oman, L. D., Pitari, G., Pozzer, A., Quaglia, I., Revell, L. E., Rozanov, E., Stenke, A., Stone, K., Strahan, S., Tilmes, S., Tost, H., Westervelt, D. M., and Zeng, G.: A machine learning examination of hydroxyl radical differences among model simulations for CCMI-1, Atmos. Chem. Phys., 20, 1341-1361, http://doi.org/10.5194/acp-20-1341-2020, 2020.

Development of the global atmospheric general circulation-chemistry model BCC-GEOS-Chem v1.0: model description and evaluation

Xiao Lu[1,2], Lin Zhang[1,*], Tongwen Wu[3,*], Michael S. Long[2], Jun Wang[4], Daniel J. Jacob[2], Fang Zhang[3], Jie Zhang[3], Sebastian D. Eastham[5], Lu Hu[6], Lei Zhu[2,7,8], Xiong Liu[7], and Min Wei[9]

(1) Laboratory for Climate and Ocean-Atmosphere Sciences, Department of Atmospheric and Oceanic Sciences, School of Physics, Peking University, Beijing 100871, China
(2) School of Engineering and Applied Sciences, Harvard University, Cambridge, MA 02138, USA
(3) Beijing Climate Center, China Meteorological Administration, Beijing 100081, China
(4) University of Iowa, Iowa City, IA 52242, USA
(5) Laboratory for Aviation and the Environment, Massachusetts Institute of Technology, Cambridge, MA 02139, USA
(6) Department of Chemistry and Biochemistry, University of Montana, Missoula, MT 59812, USA
(7) Harvard-Smithsonian Center for Astrophysics, Cambridge, MA 02138, USA
(8) School of Environmental Science and Engineering, Southern University of Science and Technology, Shenzhen 518055, Guangdong, China
(9) National Meteorological Information Center, China Meteorological Administration, Beijing 100871, China

Correspondence to Lin Zhang (zhanglg@pku.edu.cn) and Tongwen Wu (twwu@cma.gov.cn)

Abstract

Chemistry plays an indispensable role in investigations of the atmosphere, however, many climate models either ignore or greatly simplify atmospheric chemistry, limiting both their accuracy and their scope. We present the development and evaluation of the online global atmospheric chemical model BCC-GEOS-Chem v1.0, coupling the GEOS-Chem chemical transport model (CTM) as an atmospheric chemistry component in the Beijing Climate Center atmospheric general circulation model (BCC-AGCM). The GEOS-Chem atmospheric chemistry component includes detailed tropospheric HO_x-NO_x-VOC-ozone-bromine-aerosol chemistry and online dry and wet deposition schemes. We then demonstrate the new capabilities of BCC-GEOS-Chem v1.0 relative to the base BCC-AGCM model through a three-year (2012-2014) simulation with anthropogenic emissions from the Community Emissions Data System (CEDS) used in the Coupled Model Intercomparison Project Phase 6 (CMIP6). The model well captures the spatial distributions and seasonal variations in tropospheric ozone, with seasonal mean biases of 0.4-2.2 ppbv at 700-400 hPa compared to satellite observations and within 10 ppbv at the surface-500 hPa compared to global ozonesonde observations. The model has larger high ozone biases over the tropics which we attribute to an overestimate of ozone chemical production. It underestimates ozone in the upper troposphere which likely due to either the use of a simplified stratospheric ozone scheme and/or to biases in estimated stratosphere-troposphere exchange dynamics. The model diagnoses the global tropospheric ozone burden, OH concentration, and methane chemical lifetime to be 336 Tg, 1.16×10^6 molecule cm^{-3}, and 8.3 years, respectively, consistent with recent multi-model assessments. The spatiotemporal distributions of NO_2, CO, SO_2, CH_2O, and aerosols optical depth are generally in agreement with satellite observations. The development of BCC-GEOS-Chem v1.0 represents an important step for the development of fully coupled earth system models (ESMs) in China.

1. Introduction

Atmospheric chemistry plays an indispensable role in the evolution of atmospheric gases and aerosols, and is also an essential component of the climate system due to its active interactions with atmospheric physics and biogeochemistry on various spatiotemporal scales. Climate modulates the natural emissions, chemical kinetics, and transport of atmospheric gases and aerosols, while changes in many of these constituents alter the radiative budgets of the climate system and also influence the biosphere (Jacob and Winner, 2009; Fiore et al., 2012; Lu et al., 2019a). Climate-chemistry coupled models are indispensable tools to quantify climate-chemistry interactions and to predict future air quality. However, coupling transport and chemistry of hundreds of chemical species on all spatiotemporal scales in climate system models (CSMs) posts a considerable challenge for model complexity and computational resources. Only ten of the thirty-nine CSMs in the phase five of the Coupled Model Intercomparison Project (CMIP5) simulated atmospheric chemistry interactively (IPCC AR5, 2013). In the other models, including all the five Chinese CSMs, chemically active species were prescribed. Development of climate-chemistry coupled model has been identified as a research frontier for atmospheric chemistry (National Research Council, 2012), and also a priority for CSM development particularly in China. An initiative to include online simulation of atmospheric chemistry in CSM, as an essential step toward building a climate-chemistry coupled model, was launched in the Beijing Climate Center (BCC) at the China Meteorological Administration (CMA) after CMIP5.

Here we present the development of the global atmospheric chemistry-general circulation model BCC-GEOS-Chem v1.0, which enables online simulation of atmospheric chemistry in the BCC-CSM version 2 (BCC-CSM2). BCC-GEOS-Chem is built on the coupling of the GEOS-Chem chemical module to the BCC Atmospheric General Circulation Model (BCC-AGCM), the atmospheric component of the BCC-CSM2. BCC-CSM2 is a fully coupled global CSM in which the atmosphere, land, ocean, and sea-ice components interact with each other through the exchange of momentum, energy, water, and carbon (Wu et al., 2008, 2013, 2019). The earlier version of BCC-CSM (v1.1 and v1.1m) was enrolled in CMIP5 and has been widely applied on weather and climate research (e.g., Wu et al., 2013, 2014; Xin et al., 2013; Zhao and He, 2015). It has been recently updated to BCC-CSM2 and is being used in that configuration for the Coupled Model Intercomparison Project Phase 6 (CMIP6) (Wu et al., 2019). GEOS-Chem (http://geos-chem.org), originally described by Bey et al. (2001) is a global three-dimensional chemical transport model (CTM) which includes detailed state-of-science gas-aerosol chemistry, is used by a large international community for a broad range of research on atmospheric chemistry, is continually updated with scientific innovations from users, is rigorously benchmarked, and is openly accessible on the cloud (Zhuang et al., 2019). The model is continually evaluated with atmospheric observations by its user community (e.g., Hu et al., 2017). The integration of BCC-AGCM and GEOS-Chem for online simulation of global atmospheric chemistry will have attractive scientific and operational applications (e.g., sub-seasonal air quality prediction), and also represents an important step for the development of fully coupled earth system models (ESMs) in China.

Until recently, the offline GEOS-Chem CTM relied exclusively on fixed longitude-latitude grids and was designed for shared-memory (OpenMP) parallelization. With such features the GEOS-Chem CTM was not flexible to be coupled with BCC-CSM, which typically runs on spectral space (with adjustable options for the grid type and resolution dependent on the wave truncation number) and requires vast computational resources. Integration of GEOS-Chem chemical module into CSMs has been enabled by separating the module (which simulates all local processes including chemistry, deposition, and emission) from the simulation of transport, and making it operate on 1-D (vertical) columns in a grid-independent manner (Long et al., 2015; Eastham et al., 2018). The GEOS-Chem chemical module can thus be coupled with a CSM on any grid, and the CSM simulation of dynamics then handles chemical transport. GEOS-Chem used as an online chemical module in CSMs shares the exact same code as the classic offline GEOS-Chem for local processes (chemistry, deposition, and emission) (Long et al., 2015). This capability ensures that the scientific improvements of GEOS-Chem contributed from worldwide research community can be conveniently incorporated into CSMs, allowing the chemistry of BCC-GEOS-Chem to be trackable to the latest GEOS-Chem version. Previous studies have demonstrated the success of coupling GEOS-Chem into the NASA GEOS-5 Earth system model and more recently the Weather Research and Forecasting (WRF) mesoscale meteorological model as an online atmospheric chemistry module (Long et al., 2015; Hu et al., 2018; Lin et al., 2020).

This paper presents the overview of the BCC-GEOS-Chem v1.0 model, and evaluates the model simulation of present-day atmospheric chemistry. The model framework and its components are described in Section 2. We conducted a three-year (2012-2014) model simulation to demonstrate the model capability and for model evaluation. In section 3, we compare simulated gases and aerosols with satellite and *in-situ* observations, and also diagnose the global tropospheric ozone burden and budget. Future plans for model development and summary are presented in Section 4.

2. Development and description of the BCC-GEOS-Chem v1.0

Figure 1 presents the framework of the BCC-GEOS-Chem v1.0. BCC-GEOS-Chem v1.0 includes interactive atmosphere (including dynamics, physics, and chemistry) and land modules, and other components such as ocean and sea ice are configured as boundary conditions for this version. Atmospheric dynamics and physics module *(Section 2.1)* and the land module *(Section 2.2)* come from the BCC-AGCM version 3 and the BCC Atmosphere and Vegetation Interaction Model version 2 (BCC-AVIM2), respectively. Atmosphere and land modules exchange the fluxes of momentum, energy, water, and carbon through the National Center for Atmospheric Research (NCAR) flux Coupler version 5. Dynamic and physical parameters from both the atmosphere (e.g., radiation, temperature, and wind) and the land modules (e.g., surface stress and leaf area index) are then used to drive the GEOS-Chem chemistry *(Section 2.3)* and deposition *(Section 2.4)* of atmospheric gases and aerosols. Anthropogenic and biomass burning emissions are from the inventories used for the CMIP6 *(Section 2.5.1)*. A number of climate-sensitive natural emissions such as biogenic and lightning emissions are calculated online in the model (*Section 2.5.2*). Boundary conditions, external forcing, and experiment design are described in *Section 2.6*.

2.1 The atmospheric model BCC-AGCM3

BCC-AGCM3 is a global atmospheric spectral model. It has adjustable horizontal resolution and 26 vertical hybrid layers extending from the surface to 2.914 hPa. In this study we use the default horizontal spectral resolution of T42 (approximately 2.8° latitude × 2.8° longitude). The dynamical core and physical processes of the BCC-AGCM3 have been described comprehensively in Wu et al. (2008, 2010) with recent updates documented in Wu et al. (2012, 2019). Wu et al. (2019) showed that the BCC-CSM2 (BCC-AGCM3 as the atmospheric model) well captured the global patterns of temperature, precipitation, and atmospheric energy budget. BCC-CSM2 also showed significant improvements in reproducing the historical changes of global mean surface temperature from 1850s and climate variabilities such the quasi-biennial oscillation (QBO) and the El Niño–Southern Oscillation (ENSO) compared with its previous version BCC-CSM1.1m (Wu et al., 2019). Here we present a brief summary of the main features in BCC-AGCM3.

The governing equations and physical processes (e.g., clouds, precipitation, radiative transfer, and turbulent mixing) of BCC-AGCM3 are originated from the Eulerian dynamic framework of the Community Atmosphere Model (CAM3) (Collins et al., 2006), but substantial modifications have been incorporated. Wu et al. (2008) introduced a stratified reference of atmospheric temperature and surface pressure to the governing equations. In this way, prognostic temperature and surface pressure in the original governing equation can be derived from their prescribed reference plus the prognostic perturbations relative to the reference. Resolving algorithms (e.g., explicit and semi-implicit time difference scheme) were adapted accordingly. The modified dynamic framework reduced the truncation errors in the model as well as the bias due to inhomogeneous vertical stratification, and therefore improved the descriptions of the pressure gradient force and the vertical temperature structure (Wu et al., 2008). BCC-AGCM3 also implements a new mass-flux cumulus scheme to parameterize deep convection (Wu, 2012). The revised deep convection parameterization by including the entrainment of environment air into the uplifting parcel better captured the realistic timing of intense precipitation (Wu, 2012) and the Madden-Julian Oscillation (MJO) (Wu et al., 2019). Other important updates of atmospheric physical processes in BCC-AGCM3 relative to CAM3 include a new dry adiabatic adjustment to conserve the potential temperature, a modified turbulent flux parameterization to involve the effect from waves and sea spray on ocean surface latent and sensible heat, a new scheme to diagnose cloud fraction, a revised cloud microphysics scheme to include the aerosol indirect effects based on bulk aerosol mass, and modifications for radiative transfer and boundary layer parameterizations (Wu et al., 2010; 2014; 2019).

2.2 The land model BCC-AVIM2

BCC-AVIM2 is a comprehensive land surface model originated from the Atmospheric and Vegetation Interaction Model (AVIM) (Ji, 1995; Ji et al., 2008), and serves as the land component in BCC-CSM2. It includes three submodules: the biogeophysical module, plant ecophysiological module, and soil carbon-nitrogen dynamic module. The biogeophysical module simulates the transfer of energy, water, and carbon between the atmosphere, plant canopy, and soil. It has 10 soil layers and up to 5 snow layers. The ecophysiological module describes the ecophysiological activities such as photosynthesis, respiration, turnover, and mortality of vegetation, and diagnoses the induced changes of biomass. The soil carbon-nitrogen dynamic module describes the biogeochemical process such as the conversion and decomposition of soil organic carbon. The vegetation surface in BCC-AVIM2 is divided into 15 plant functional types (PFTs) as shown in Table 1, and each grid cell contains up to 4 PFTs types. Wu et al. (2013) showed that the model well captured the spatial distributions, long-term trends, and interannual variability of global carbon sources and sinks compared to observations and other models. Recent improvements in BCC-AVIM2, such as the introduction of a variable temperature threshold for the thawing/freezing of soil water, and improved presentations of snow surface albedo and snow cover fraction, are described in Li et al. (2019). Biogenic emissions and dust mobilizations are also implemented in BCC-AVIM2 interactively with the atmosphere, as will be described later in Section 2.5.

2.3. Atmospheric chemistry

We implement in this study the GEOS-Chem v11-02b "Tropchem" mechanism as the atmospheric chemistry module of BCC-GEOS-Chem v1.0. As described in the introduction, GEOS-Chem used as an online chemical module in ESMs shares the exact same codes for local terms (chemistry, deposition, and emission) as the classic offline GEOS-Chem. Here, we use the GEOS-Chem chemical module to process chemistry and deposition in BCC-GEOS-Chem v1.0, and operate emission separately in the model as will be described in Section 2.5.

GEOS-Chem v11-02b "Tropchem" mechanism describes advanced and detailed HO_x-NO_x-VOC-ozone-bromine-aerosol chemistry relevant to the troposphere (Mao et al., 2010, 2013; Parrella et al., 2012; Fischer et al., 2014; Marais et al., 2016). It includes 74 advected species (tracers) and 91 non-advected species (http://wiki.seas.harvard.edu/geos-chem/index.php/Species_in_GEOS-Chem). Tracer advection in BCC-GEOS-Chem v1.0 is performed using a semi-Lagrangian scheme (Williamson and Rasch, 1989), and the vertical diffusion within the boundary layer follows the parameterization of Holtslag and Boville (1993). Photolysis rates are calculated by the Fast-JX scheme (Bian and Prather, 2002). The simulation of sulfate-nitrate-ammonia (SNA) aerosol chemistry, four-size bins of mineral dust (radii of 0.1-1.0, 1.0-1.8, 1.8-3.0, and 3.0-6.0 μm), and two types of sea salt aerosols (accumulating mode: 0.01-0.5; coarse mode: 0.5-8.0 μm) follows Park et al. (2004), Fairlie et al. (2007), and Jaegle et al. (2011). Aerosol and gas-phase chemistry interacts through heterogeneous chemistry on aerosol surface (Jacob, 2000; Evans and Jacob, 2005; Mao et al., 2013), aerosol effects on photolysis (Martin et al., 2003), and gas-aerosol partitioning of NH_3 and HNO_3 calculated by the ISORROPIA II thermodynamic module (Fontoukis and Nenes, 2007; Pye et al., 2009). Methane concentrations in the chemistry module are prescribed as uniform mixing ratios over four latitudinal bands (90°–30°S, 30°S–0°, 0°–30°N, and 30°–90°N), with the year-specific annual mean concentrations given by surface measurements from the NOAA Global Monitoring Division. Stratospheric ozone is calculated by the linearized ozone parameterization (LINOZ) (McLinden et al., 2000) and is transported to the troposphere driven by the model wind fields.

2.4. Dry and wet deposition

Dry and wet deposition for both gas and aerosols are parameterized following GEOS-Chem algorithms. Dry deposition is calculated online based on the resistance-in-series scheme (Wesely, 1989). The scheme describes gaseous dry deposition by three separate processes, *i.e.*, the turbulent transport in aerodynamic layer, molecular diffusion through the quasi-laminar boundary layer, and uptake at the surface. Aerosol dry deposition further considers the gravitational settling of particles as described in Zhang et al. (2001). Variables needed for the dry deposition calculation such as the friction velocity, Monin-Obukhov length, and leaf area index (LAI) are obtained from the atmospheric dynamics/physics modules or the land module BCC-AVIM, based on which ~~then~~ GEOS-Chem calculates the aerodynamic, boundary-layer, and surface resistances. The impacts of some other short-term land variables, such as ~~modelled~~ stomatal conductance, on dry deposition are not ~~considered~~included yet. We have also reconciled the land use types (LUT) used in dry deposition with those used in BCC-AVIM, following Geddes et al. (2016) and Zhao et al. (2017). The LUTs from BCC-AVIM are mapped directly to the 11 deposition surface types used that in GEOS-Chem as shown in Table 1. Dry deposition velocity is calculated as the weighted average over all LUTs in each grid box.

Wet deposition of aerosols and soluble gases by precipitation in BCC-GEOS-Chem v1.0 includes the scavenging in convective updrafts, in-cloud rainout, and below-cloud washout (Liu et al., 2001). Following the implementation of GEOS-Chem chemical module to GEOS-5 ESM (Hu et al., 2018), convective transport of chemical tracers and scavenging in the updrafts in BCC-GEOS-Chem v1.0 is performed using the GEOS-Chem convection scheme but with convection variables diagnosed from BCC-AGCM. This takes advantages of the existing capability of the GEOS-Chem scheme to describe gas and aerosol scavenging (Liu et al., 2001; Amos et al., 2012).

2.5 Emissions

2.5.1 Offline emissions

Historical anthropogenic emissions used in this study are mostly obtained from the Community Emissions Data System (CEDS) emission inventory (Hosely et al., 2018). CEDS is an updated global emission inventory which provides sectoral, gridded, and monthly emissions of reactive gases and aerosols from 1750-2014 for use in the CMIP6 experiment (Eyring et al. 2016; Hosely et al., 2018). Here we use the CEDS anthropogenic emissions of NO_x, CO, SO_2, NH_3, non-methane volatile organic compounds (NMVOCs), and carbonaceous aerosols (black carbon (BC) and organic carbon (OC)) (Table 2). We also include three-dimensional aircraft emissions of several gases and aerosols in the model. The historical global biomass burning emission inventory is obtained from van Marle et al. (2017) which is also used for the CMIP6 experiment. We also incorporate emissions from the Atmospheric Chemistry and Climate Model Intercomparison Project (ACCMIP) inventory (http://accent.aero.jussieu.fr/ACCMIP.php, last access: 14 Jun 2020; Lamarque et al., 2010) and from Wu et al. (2020) for emissions not included in CEDS data set. These mainly apply to oceanic emissions, soil NO_x emissions, and volcanic SO_2 emissions. Several sources (e.g. oceanic acetaldehyde emissions (Millet et al., 2010; Wang et al., 2019)) have not yet been included in ~~our~~this model ~~simulation~~version.~~Prescribed soil NO_x, volcano SO_2, and ocean dimethyl sulfide (DMS) emissions from the CMIP5 dataset are also included.~~

Table 2 lists the amount of annual total emissions of chemicals used in this study separated by emission sectors averaged over 2012-2014. Figure 2a and 2b shows the spatial distributions of annual NO (not including lightning emissions which will be discussed below separately) and CO emissions. Global annual total emissions of NO (not including lightning emissions) and CO are 111.1 and 925.5 Tg year^{-1}, respectively. The global anthropogenic emissions are relatively flat in 2012-2014 (e.g. from 614.7 to 619.6 Tg year^{-1} for CO), while the biomass burning emissions have much stronger interannual variability (e.g., varying from 209 to 256 Tg year^{-1} for CO). As pointed out by Hosely et al. (2018), CEDS anthropogenic emissions are generally higher than previous inventories. For instance, the anthropogenic NO_x and CO emissions are, respectively, about 10% and 8% higher compared to CMIP5 emissions in 1980-2000 periods. This is likely due to the updates of emission factors and inclusions of new emission sectors (Hosely et al., 2018). Compared to CMIP5, biomass burning emissions used in CMIP6 for the 2000 condition is about 20% and 30% lower for CO and OC, respectively, but is about 17% higher for NO_x (Fig. 13 in van Marle et al., 2017).

2.5.2 Online emissions

BCC-GEOS-Chem v1.0 includes a number of climate-sensitive natural sources. Biogenic emissions of NMVOCs are calculated online using the Model of Gases and Aerosols (MEGAN) algorithm (Guenther et al., 2012) in the land module. MEGAN estimates biogenic emissions as a function of an emission factor at standard condition, a normalized emission activity factor relative to the standard condition, and a scaling ratio which accounts for canopy production and loss. The emission activity factor is further determined by surface or plant parameters such as leaf age and LAI diagnosed in BCC-AVIM, as well as meteorological variables such as radiation and temperature. The annual biogenic isoprene emissions calculated in BCC-GEOS-Chem v1.0 are 410.0 Tg year^{-1} averaged for 2012-2014 period with a relatively small interannual variability (404.6 to 415.2 Tg year^{-1}). This is close to but lower than estimates from the literature (500-750 Tg, Guenther et al., 2012). The model captures the hot spots of biogenic isoprene emissions in the tropical continents and the southeastern US (Fig. 2c).

Parameterization of lightning NO emissions follows Price and Rind (1992). The model diagnoses the lightning flash frequency in deep convection as a function of the maximum cloud-top-height (CTH). Lightning NO production is then calculated as a function of lightning flash frequency, fraction of intracloud (IC) and cloud-to-ground (CG) lightning based on the cloud thickness, and the energy per flash (Price et al., 1997). Vertical distributions of lightning NO emissions in the column follow Ott et al. (2010). The model estimates ~~t~~global annual total lighting NO emissions of 10.9 to 12.2 Tg NO year^{-1} for 2012-2014, in agreement with the best estimate of present-day emissions (10.7±6.4 Tg NO year^{-1} as summarized in Schumann and Huntrieser, 2007). The emissions are centered near the tropics due to strong convection as shown in Figure 2d.

The model also includes wind-driven sea salt and mineral dust emissions. Emission fluxes of sea salt aerosols are dependent on the sea salt particle radius and proportional to the 10-meter wind speed with a power of 3.41 following the empirical parameterization from Monahan et al. (1986) and Gong et al. (1997). Mineral dust emissions are determined by wind friction speed, soil moisture, and vegetation type following the Dust Entrainment and Deposition (DEAD) scheme as described by Zender et al. (2003). Figure 2e and 2f show the spatial distributions of sea salt and mineral dust emissions, with their annual total emissions of 3963 Tg and 1347 Tg, respectively, consistent with previous estimates from Jaeglé et al. (2011) and Fairlie et al. (2007).

2.6 Boundary conditions, external forcing, and experiment design

BCC-GEOS-Chem v1.0 is configured using prescribed ocean and sea ice as boundary conditions. Historical sea surface temperature and sea-ice extents are obtained from (https://esgf-node.llnl.gov/search/input4mips/, last access: 2 June 2019). These prescribed datasets are also used in CMIP6 atmosphere-only simulations. External forcing data, including historical greenhouse gas concentrations (CO_2, CH_4, N_2O, CFCs) (Meinshausen et al., 2017), land use forcing, and solar forcing, are also accessed from (https://esgf-node.llnl.gov/search/input4mips/). BCC-CSM2 has implemented the radiative transfer effects of greenhouse gases and aerosols as well as the aerosol-cloud interactions based on bulk aerosol mass concentrations (Wu et al., 2019). Since BCC-CSM2 does not include interactive atmospheric chemistry, the calculation of radiative transfer and aerosol-cloud interactions are based on historical gridded ozone concentrations from CMIP5 and CMIP6-recommended anthropogenic aerosol optical properties (Stevens et al., 2017). Here for BCC-GEOS-Chem v1.0, we follow BCC-CSM2 and use these prescribed ozone and aerosols rather than model online calculated values for feedback calculation. This is meant to focus on modeling and evaluation of atmospheric chemistry in this work as the first step of the coupling. Interactive coupling of chemistry and climate through radiation and aerosol-cloud interactions will be considered in the next version of BCC-GEOS-Chem.

We conduct BCC-GEOS-Chem v1.0 simulations from 2011 to 2014. The initial conditions for atmospheric dynamics and physics at 2011 are obtained from the historical simulations (1850-2014) of BCC-CSM2 (Wu et al., 2019), and initial states of chemical tracers are obtained from the GEOS-Chem Unit Tester (http://wiki.seas.harvard.edu/geos-chem/index.php/Unit_Tester_for_GEOS-Chem_12, last access: 2 June 2019). Model results for 2012-2014 are evaluated.

3. Model evaluation

3.1 Observations used for model evaluation

We use an ensemble of surface, ozonesonde, and satellite observations to evaluate the BCC-GEOS-Chem v1.0 simulation of present-day atmospheric chemistry (Table 3). Ozonesonde measurements are obtained from the World Ozone and Ultraviolet Radiation Data Centre (WOUDC; http://woudc.org/data.php, last access: 2 June 2019) operated by the Meteorological Service of Canada. The network also includes sites from the Southern Hemisphere Additional Ozonesondes (SHADOZ, Thompson et al., 2003). To derive the monthly mean ozone profiles, only sites and months with more than three observations ~~in the~~per month are considered, and simulated monthly mean ozone profiles are sampled over the corresponding model grids (Lu et al., 2019b). We further categorize the WOUDC observations into ten~~nine~~ regions following Tilmes et al. (2012) and Hu et al. (2017) for model evaluation as shown in Figure 3. We also use the TOAR surface ozone database (Schultz et al., 2017a) that provides ozone metrics (e.g. monthly mean) for more than 9000 monitoring sites around the world from the 1970s to 2014 (Schultz et al., 2017b). Surface aerosol measurements (sulfate, nitrate, OC, BC) over the US are obtained from the Interagency Monitoring of Protected Visual Environments (IMPROVE) network. These aerosol measurements are 24-hour averages every 3 days.

Satellite products from the NASA Earth Observing System (EOS) Aura satellite's Ozone Monitoring Instrument (OMI) are also used. We use the OMI PROFOZ ozone profiles with 24 layers extending from the surface to 60 km retrieved by Liu et al. (2005; 2010) based on the optimal estimation technique (Rodgers, 2000). The OMI PROFOZ dataset has been comprehensively validated by comparisons with ozonesondes (Zhang et al., 2010; Hu et al., 2017; Huang et al., 2017) and satellite products (Huang et al., 2018). We also use the OMI gridded monthly mean tropospheric column of nitrogen dioxide (NO_2) (Krotkov et al., 2013), formaldehyde (CH_2O) (De Smedt et al., 2015), and planetary boundary layer (PBL) sulfur dioxide (SO_2) column (Krotkov et al., 2015). Other satellite observations include ~~total column~~ carbon monoxide (CO) observations from Measurements of Pollution in the Troposphere (MOPITT) (Deeter et al., 2017), and aerosol optical depth (AOD) at 550 nm from the Moderate Resolution Imaging Spectroradiometer (MODIS) (available at https://neo.sci.gsfc.nasa.gov/view.php?datasetId=MODAL2_M_AER_OD, last access: 2 June 2019). Satellite observations are further re-gridded to the model resolution for model evaluation, except for the MODIS AOD dataset due to a large number of invalid measurements.

3.2 Evaluation of tropospheric ozone with observations

Figure 4 shows the spatial and seasonal distributions of mid-tropospheric ozone (700-400 hPa) from OMI satellite observations and BCC-GEOS-Chem v1.0 simulation averaged over 2012-2014, as well as their differences. We analyze ozone at 700-400hPa where OMI satellite has the peak sensitivity (Zhang et al., 2010). Model outputs are sampled along the OMI tracks and smoothed with OMI averaging kernels for proper comparison to the observations (Zhang et al., 2010; Hu et al., 2017, 2018; Lu et al., 2018).

The model well captures the main features of tropospheric ozone distribution and seasonal variation. Both satellite observations and BCC-GEOS-Chem v1.0 model results show high mid-tropospheric ozone levels over the northern mid-latitudes in boreal spring due to stronger stratospheric influences and in summer due to higher photochemical production, and over the Atlantic and southern Africa during boreal autumn driven by strong biomass burning emissions (Fig. 2), lightning NOx and dynamical processes (e.g., Sauvage et al., 2007). The spatial patterns of observed and simulated tropospheric ozone values are highly correlated, with correlation coefficients (r) of 0.79-0.93. BCC-GEOS-Chem v1.0 shows small global seasonal mean biases of 0.4~2.2 ppbv relative to OMI observations, comparable to the biases of 0.1~2.7 ppbv for G5NR-Chem (NASA GEOS-ESM with GEOS-Chem v10-01 as an online chemical module) in a similar period (Hu et al., 2018). We find that BCC-GEOS-Chem v1.0 tends to overestimate tropospheric ozone levels over tropical oceans by 3-12 ppbv and underestimate ozone over the northern mid-latitudes by 3-9 ppbv, similar to the patterns simulated by the classic GEOS-Chem and G5NR-Chem models (Hu et al., 2017, 2018).

Comparisons with global ozonesonde observations further demonstrate that BCC-GEOS-Chem v1.0 has no significant biases in the tropospheric ozone simulation. As shown in Figure 5, the model well reproduces the observed annual mean ozone vertical structures, e.g., the slow increase of ozone with increasing altitude in the troposphere, and the sharp ozone gradient near and above the tropopause. Figure 6 compares seasonal variations of ozone concentrations in different regions at three tropospheric levels (800 hPa, 500 hPa, and 300 hPa). Overall, the model reproduces the ozone annual cycles driven by different chemical and dynamical processes. The model captures the springtime and summertime ozone peaks at the northern mid-latitudes (Japan, US, Europe, Canada) (*r*=0.53~0.94 for different layers), but only fairly reproduces the annual ozone cycle in the Southern Hemisphere (SH) and the tropics. Mean model biases at the three layers are mostly within 10 ppbv, with small low biases over the northern mid-latitudes (~~-6.2~-0.8~~ -6.0~-0.6 ppbv), and high biases over the tropics in the lower and middle troposphere (e.g., about 10 ppbv at 800 hPa over the SH tropics), consistent with the comparison with satellite observations (Fig.4). We find that the model has large low ozone bias in the upper troposphere (300 hPa) particularly over the northern polar regions (~-30 ppbv). The underestimation extends to the stratosphere globally except for the extratropical Southern Hemisphere (Fig. 5). These negative model biases are likely due to the use of a simplified stratospheric ozone scheme and/or errors in modeling dynamics of ozone exchange between the stratosphere and the troposphere as will be discussed later, or the low model vertical resolution (26 layers).

Figure 7 compares the simulated ground-level ozone with more than 300 rural/remote sites (defined by a number of metrics including population density and nighttime lights data, Schultz et al., 2017b) around the world from the TOAR database. We average all observations within the same model grid square for statistical analyses, a recommended way for evaluating coarse-resolution chemical models (Cooper et al., 2020). BCC-GEOS-Chem v1.0 captures the spatial and seasonal distributions of global ground-level ozone with *r* ranging from 0.53 to 0.59 (N=154). The annual mean model biases are 4.9 ppbv (15%) for all observations, with larger high bias in June-July-August period (11.0 ppbv, 32%). Inclusion of urban and suburban sites slightly decreases the spatial correlations (*r*=0.34~0.60, N=292) and enlarges the annual mean high bias (10.2 ppbv). We find again that the high biases are more prominent in the tropics (e.g., coastal sites in the western Pacific and Indonesia) and in summer. Although the above comparison is heavily weighted toward the US, Europe, Japan and South Korea due to the density of observations in these regions, our results demonstrate the overall good performance for BCC-GEOS-Chem v1.0 in simulating ground-level ozone at least for rural and remote regions.

3.3 Tropospheric ozone and OH budgets in BCC-GEOS-Chem v1.0

We then diagnose the global tropospheric ozone burden and its driving terms (Table 4 and Figure 8). BCC-GEOS-Chem v1.0 estimates the global tropospheric ozone burden to be 336.0 Tg averaged over 2012-2014. This is consistent with the results from the classic offline GEOS-Chem CTM and the G5NR-Chem (~350 Tg) with an earlier version (v10-01) of GEOS-Chem as chemical module (Hu et al., 2017; 2018), and also in agreement with the recent model assessments of 49 models (320-370 Tg, Young et al., 2018). We divide the global tropospheric ozone burden into different regions following Young et al. (2013) as shown in Figure 8a and 8b. We find that the overall distributions of ozone burden are consistent with the ensemble of 15 models from the Atmospheric Chemistry and Climate Model Intercomparison Project (ACCMIP) (Young et al., 2013). The main discrepancy between BCC-GEOS-Chem v1.0 and ACCIMIP occurs within 30S-30°N. ACCMIP results show that ozone over 30°S-30°N and below 250 hPa accounts for 36.9% of the global tropospheric ozone burden, while BCC-GEOS-Chem v1.0 shows a higher proportion (48.5%). While ozone overestimation of BCC-GEOS-Chem v1.0 over 30°S-30°N is also seen from the comparisons to observations as discussed previously, the discrepancy between our results and ACCMIP model ensemble mean is also likely due to the different simulation year (2000 conditions for ACCMIP versus 2012-2014 for BCC-GEOS-Chem v1.0). Zhang et al. (2016) showed that the equatorward redistribution of anthropogenic emissions significantly increased the global tropospheric ozone burden from 1980 to 2010, with the largest enhancements over the tropics. BCC-GEOS-Chem v1.0 underestimates the proportion of ozone burden in the upper troposphere (5.1%-10.9%) compared to the ACCMIP results (6.4-15.2%), again likely reflecting the model limitation in simulating stratosphere ozone and/or its exchange with the troposphere.

We find that the global tropospheric mean OH concentration in BCC-GEOS-Chem v1.0 is 1.16×10^6 molecule cm^{-3}, close to the offline GEOS-Chem v10-01 (1.25×10^6 molecule cm^{-3}, Hu et al., 2018) and well within the range of 16 ACCMIP models (1.11±0.16×10^6 molecule cm^{-3}, Naik et al., 2013). Figure 8c and 8d compares the distribution of simulated OH concentrations with the climatology derived from previous studies (Spivakovsky et al., 2001; Emmons et al., 2010). We find that the model shows notable high bias in the lower troposphere (below 750 hPa) particularly in the tropics (2.04 to 2.45 molecule cm^{-3} in BCC-GEOS-Chem v1.0 compared to 1.44 to 1.52 molecule cm^{-3} in Spivakovsky et al., 2001). Discrepancies in modeling climate and concentrations of methane, ozone, NO_x, and CO can all contribute to the OH bias in climate-chemistry models (Nicely et al., 2020).~~This discrepancy appears to be mainly driven by the high bias in ozone levels in this region. Furthermore, w~~We calculate the methane chemical lifetime against OH loss to be 8.3 years in BCC-GEOS-Chem v1.0, which falls in the low end of the range reported from ACCMIP multi-model assessments (9.7±1.5 years) (Naik et al., 2013).

We now diagnose the budget of global tropospheric ozone in BCC-GEOS-Chem v1.0. Following the classic GEOS-Chem, BCC-GEOS-Chem v1.0 diagnoses the chemical production and loss of the odd oxygen family (O_x, including O_3, NO_2, NO_y, several organic nitrates and bromine species) to account for the rapid cycling among O_x constituents. Ozone accounts for more than 95% of the total O_x (Hu et al., 2017). The global annual ozone chemical production and loss are 5486 Tg and 4983 Tg, respectively (Table 4); both are higher than the classic GEOS-Chem (Hu et al., 2017) and fall in the high quartile of multi-model assessments (Young et al., 2018). The high tropospheric ozone production is due at least in part to the high precursor emissions used in this study particularly for NO_x emissions The model shows strong chemical production over northern mid-latitude continents in summertime, and large chemical loss over the tropical oceans driven by high water vapor content (figure not shown).

The global annual mean ozone dry deposition flux diagnosed in BCC-GEOS-Chem v1.0 is 873 Tg averaged for 2012-2014. It is consistent with recent reviews by Hardacre et al. (2015) and Young et al. (2018) (700-1500 Tg from 33 model estimates). Figure 9 presents the global ozone dry deposition velocity and flux for January and July 2012-2014. Both hemispheres show larger ozone dry deposition velocities in summer than winter due to stronger atmospheric turbulence and larger vegetation cover. Large ozone dry deposition velocity (> 0.5 cm s^{-1}) can be seen over the tropical continents, while over the oceans and glaciers ozone dry deposition is very weak.

We then diagnose the annual amount of ozone stratosphere-troposphere exchange (STE) of 370 Tg as the residual of mass balance between tropospheric chemical production, chemical loss, and deposition as previous studies did (Lamarque et al., 2012; Hu et al., 2017). This value is lower than most of other model estimates (400-680 Tg, Young et al., 2018). The low STE in BCC-GEOS-Chem v1.0 appears to be the main factor causing ozone underestimates in the upper troposphere as seen above. This may reflect a number of model limitations, for example, the representation of stratospheric chemistry, inadequate STE due to model meteorology (e.g., biases in wind and tropopause), and the low model vertical resolution. Given the tropospheric ozone burden and its loss to chemistry and deposition, we derive the lifetime of tropospheric ozone of 20.9 days, consistent with the multi-model estimates (Young et al., 2013).

3.4 Evaluation of other atmospheric constituents

~~Figure 10 compares the model simulated spatial distributions of annual mean simulated NO_2, SO_2, CO, and CH_2O with satellite observations. Here we do not apply the averaging kernels to smooth modeled results, and therefore mainly focus the comparisons on spatial variations rather than absolute magnitudes. As shown in Figure 10, BCC-GEOS-Chem v1.0 captures the observed hotspots of tropospheric NO_2 and PBL SO_2 columns over the East Asia that generally follow the~~

~~distribution of anthropogenic sources. The sharp land-ocean gradients for both tracers reflect their short chemical lifetime. The spatial correlations between observations and model results are 0.87 for NO_2 and 0.52 for SO_2. The model reproduces the large total CO column over the northern mid-latitudes driven by higher anthropogenic sources, and over the central Africa driven by biomass burning emissions (r=0.95). High levels of tropospheric CH_2O column are simulated over the Amazon, the central Africa, tropical Asia, and the southeastern US, typical regions where CH_2O oxidized from large biogenic emissions of VOCs (r=0.67). More assessments are required to correct the biases of these gaseous pollutants.~~

Figure 10 compares the spatial distributions of annual mean simulated CO, NO_2, SO_2, and CH_2O with satellite observations. We evaluate CO at 700 hPa where MOPITT satellite has generally high sensitivity (Emmons et al., 2004; Pfister et al., 2005), and apply averaging kernel to smooth the modelled CO. As shown in Figure 10, BCC-GEOS-Chem v1.0 reproduces the high CO levels over the northern mid-latitudes driven by higher anthropogenic sources, and over the central Africa driven by biomass burning emissions (spatial correlation coefficient r=0.92)~~, but shows~~ with some overestimates~~ion~~. It also captures the observed hotspots of tropospheric NO_2 (r=0.87) and PBL SO_2 columns (r=0.32) over the East Asia that generally follow the distribution of anthropogenic sources. The sharp land-ocean gradients for both tracers reflect their short chemical lifetime. We find low biases in the modelled PBL SO_2 especially over the volcanic eruption regions (e.g., Central Africa) but high biases in the industrialized regions such as East Asia, a pattern consistent with previous comparisons between the OMI and GEOS-Chem PBL SO2 columns, which may reflect inappropriate ship and volcanic emissions in the model (Lee et al., 2009) and/or the model bias in the PBL height. High levels of tropospheric CH_2O column are simulated over the Amazon, the central Africa, tropical Asia, and the southeastern US, typical regions where CH_2O oxidized from large biogenic emissions of VOCs (r=0.67), but the model shows notable overestimates~~ion~~. Previous studies (Zhu et al., 2016; 2020) showed that satellite CH_2O retrievals are biased low by 20–51% compared to aircraft measurements which would partly explain the model bias. ~~More~~Future assessments are required to correct the biases of these gaseous pollutants.

We evaluate model simulated AOD at 550 nm with the MODIS AOD observations in Figure 11. High AOD values over the East Asia due to high anthropogenic emissions, and over Africa and the adjacent oceans due to dust emissions are shown in both MODIS observations and BCC-GEOS-Chem v1.0, although the model tends to underestimate the observed hotspots likely due to the coarse model resolution. Figure 12 further shows the comparison of simulated surface aerosol components (sulfate, nitrate, OC and BC) with the observations from the IMPROVE network over the US. The model fairly reproduces the spatial and seasonal patterns for all analyzed aerosol components, e.g., high sulfate and nitrate concentrations over the eastern US. Among all the components, the simulation of sulfate in the US shows best agreement with biases of -10%~20% and spatial correlation coefficients of 0.76-0.87 over model grids covering the measurement sites (N=77). The model also captures the high summertime OC and BC concentrations in the mid-western US driven by active wildfire activities (r=0.20-0.57 for different seasons). However, the model shows high biases in wintertime nitrate in the eastern US as found in previous GEOS-Chem evaluations (Zhang et al., 2012).

4. Summary and future plans

This study describes the framework and evaluation of the new global atmospheric general circulation-chemistry model BCC-GEOS-Chem v1.0. The development of the BCC-GEOS-Chem v1.0 takes advantage of grid-independent structure of the GEOS-Chem chemical module, which allows the exact same GEOS-Chem chemistry and deposition algorithms to be performed on any external grid and supported by MPI. BCC-GEOS-Chem v1.0 includes interactive atmospheric and land modules. It simulates the evolution of atmospheric chemical interactive constituents through a detailed mechanism of HO_x-NO_x-VOCs-ozone-bromine-aerosol tropospheric chemistry as well as online wet and dry deposition schemes. The model also implements a number of climate-sensitive natural emissions such as biogenic VOCs and lighting NO.

We conduct a three-year (2012-2014) model simulation with year-specific CMIP6 anthropogenic and biomass burning emissions. We evaluate the model with a focus on tropospheric ozone using surface, ozonesonde, and satellite observations. We show that BCC-GEOS-Chem v1.0 can well capture the spatial distributions (r=0.79~0.93 with OMI satellite observations of ozone at 700-400hPa) and seasonal cycles of tropospheric ozone. The model shows no significant biases in the lower and middle tropospheric ozone compared to satellite observations (0.4~2.2 ppbv at 700-400 hPa), ozonesonde (within 10 ppbv at 800, 500, and 300 hPa except for the polar upper troposphere), and surface measurements (4.9 ppbv). We calculate a global tropospheric ozone burden of 336 Tg year^{-1} and OH burden of 1.16×10^{6} molecule cm^{-3}; both are well within the ranges reported by previous studies. Regionally, the model shows notable high biases in ozone over the tropics and low ozone biases in the upper troposphere. Model diagnostics show that BCC-GEOS-Chem v1.0 has higher tropospheric ozone chemical production and loss compared to the classic GEOS-Chem but still falls in the range of previous estimates. Comparisons of other air pollutants including NO_2, SO_2, CO, CH_2O, and aerosols show reasonable agreements, with biases likely due to uncertainties in emissions.

The development of BCC-GEOS-Chem v1.0 for online atmospheric chemistry simulation represents an important step for the development of fully-coupled earth system models in China. There are still several limitations in this version that should be addressed in future model development. The current version of BCC-GEOS-Chem does not include full stratospheric chemistry mechanism, which is important for accurately modeling the evolution of ozone and its climate influences (Lu et al., 2019a). We plan to implement the unified tropospheric-stratospheric chemistry extension (UCX) (Eastham et al., 2014), which is now the "Standard" mechanism for GEOS-Chem chemistry, into the next version of BCC-GEOS-Chem. Diagnosing radiative transfer and aerosol-cloud interactions will be the next priority for model evaluation, and it can take advantage of the GEOS-Chem aerosol microphysics module (TwO-Moment Aerosol Sectional (TOMAS) module (Kodros and Pierce, 2017) or Advanced Particle Microphysics (APM) (Yu and Luo, 2009)). Updates of emissions (e.g., application of new or regional anthropogenic emissions inventories) could be merged to BCC-GEOS-Chem with the future implementation of the GEOS-Chem emission module (Harvard-NASA Emissions Component, HEMCO) (Keller et al., 2014). BCC-GEOS-Chem is ready to be updated to higher horizontal and vertical resolution of T106 (about 110km, 46 layers up to 1.5hPa) or T266 (about 45 km, 56 layers up to 0.09 hPa) with recent BCC-CSM-MR and BCC-CSM-HR (Wu et al., 2019), which enables applications on air quality prediction in the future.

Code and data availability

The GEOS-Chem model is maintained at the Harvard Atmospheric Chemistry Modeling group (http://acmg.seas.harvard.edu/geos/). The source code of BCC-GEOS-Chem v1.0 can be accessed at a DOI repository https://doi.org/10.5281/zenodo.3475649, and model outputs for 2012-2014 are available at https://doi.org/10.5281/zenodo.3496777. All source code and data can also be accessed by contacting the corresponding authors Lin Zhang (zhanglg@pku.edu.cn) and Tongwen Wu (twwu@cma.gov.cn).

Author Contributions

Lin Zhang, Tongwen Wu, Daniel Jacob, and Jun Wang led the project. Xiao Lu, Lin Zhang, Tongwen Wu, Michael Long, Fang Zhang and Jie Zhang developed the model source code. Xiao Lu performed model simulations, analyzed data, and prepared the figures with suggestions from all authors. Xiao Lu, Lin Zhang, Tongwen Wu, Daniel Jacob wrote the paper. All authors contributed to the discussion and improvement of the paper.

Competing interests

The authors declare that they have no conflict of interest.

Acknowledgement

This work is supported by the National Key Research and Development Program of China (2017YFC0210102) and the National Natural Science Foundation of China (41922037). This work is also supported by a grant to the Harvard-China Project on Energy, Economy and Environment from the Harvard Global Institute. Xiao Lu also acknowledges support from the Chinese Scholarship Council.~~and the Harvard China Project. Xiao Lu is also supported by the Chinese~~

~~Scholarship Council.~~

Reference

Bey, I., Jacob, D. J., Yantosca, R. M., Logan, J. A., Field, B. D., Fiore, A. M., Li, Q., Liu, H. Y., Mickley, L. J., and Schultz, M. G.: Global modeling of tropospheric chemistry with assimilated meteorology: Model description and evaluation, J. Geophys. Res., 106, 23073-23095, http://doi.org/10.1029/2001jd000807, 2001.

Bian, H., and Prather, M. J.: Fast-J2: Accurate Simulation of Stratospheric Photolysis in Global Chemical Models, Journal of Atmospheric Chemistry, 41, 281-296, http://doi.org/10.1023/a:1014980619462, 2002.

Cooper, O. R., Schultz, M. G., Schroeder, S., Chang, K.-L., Gaudel, A., Benítez, G. C., Cuevas, E., Fröhlich, M., Galbally, I. E., Molloy, S., Kubistin, D., Lu, X., McClure-Begley, A., Nédélec, P., O'Brien, J., Oltmans, S. J., Petropavlovskikh, I., Ries, L., Senik, I., Sjöberg, K., Solberg, S., Spain, G. T., Spangl, W., Steinbacher, M., Tarasick, D., Thouret, V., and Xu, X.: Multi-decadal surface ozone trends at globally distributed remote locations, Elem Sci Anth, 8, 23, http://doi.org/10.1525/elementa.420, 2020.

Collins, W. D., Rasch, P. J., Boville, B. A., Hack, J. J., McCaa, J. R., Williamson, D. L., Briegleb, B. P., Bitz, C. M., Lin, S.-J., and Zhang, M.: The Formulation and Atmospheric Simulation of the Community Atmosphere Model Version 3 (CAM3), J. Clim., 19, 2144-2161, http://doi.org/10.1175/jcli3760.1, 2006.

Council, N. R.: A National Strategy for Advancing Climate Modeling, The National Academies Press, Washington DC, USA, http://doi.org/10.17226/13430, 2012.

De Smedt, I., Stavrakou, T., Hendrick, F., Danckaert, T., Vlemmix, T., Pinardi, G., Theys, N., Lerot, C., Gielen, C., Vigouroux, C., Hermans, C., Fayt, C., Veefkind, P., Müller, J. F., and Van Roozendael, M.: Diurnal, seasonal and long-term variations of global formaldehyde columns inferred from combined OMI and GOME-2 observations, Atmos. Chem. Phys., 15, 12519-12545, http://doi.org/10.5194/acp-15-12519-2015, 2015.

Deeter, M. N., Edwards, D. P., Francis, G. L., Gille, J. C., Martínez-Alonso, S., Worden, H. M., and Sweeney, C.: A climate-scale satellite record for carbon monoxide: the MOPITT Version 7 product, Atmospheric Measurement Techniques, 10, 2533-2555, http://doi.org/10.5194/amt-10-2533-2017, 2017.

Eastham, S. D., Weisenstein, D. K., and Barrett, S. R. H.: Development and evaluation of the unified tropospheric–stratospheric chemistry extension (UCX) for the global chemistry-transport model GEOS-Chem, Atmos. Environ., 89, 52-63, http://doi.org/10.1016/j.atmosenv.2014.02.001, 2014.

Eastham, S. D., Long, M. S., Keller, C. A., Lundgren, E., Yantosca, R. M., Zhuang, J., Li, C., Lee, C. J., Yannetti, M., Auer, B. M., Clune, T. L., Kouatchou, J., Putman, W. M., Thompson, M. A., Trayanov, A. L., Molod, A. M., Martin, R. V., and Jacob, D. J.: GEOS-Chem High Performance (GCHP v11-02c): a next-generation implementation of the GEOS-Chem chemical transport model for massively parallel applications, Geoscientific Model Development, 11, 2941-2953, http://doi.org/10.5194/gmd-11-2941-2018, 2018.

Emmons, L. K., Deeter, M. N., Gille, J. C., Edwards, D. P., Attié, J. L., Warner, J., Ziskin, D., Francis, G., Khattatov, B., Yudin, V., Lamarque, J. F., Ho, S. P., Mao, D., Chen, J. S., Drummond, J., Novelli, P., Sachse, G., Coffey, M. T., Hannigan, J. W., Gerbig, C., Kawakami, S., Kondo, Y., Takegawa, N., Schlager, H., Baehr, J., and Ziereis, H.: Validation of Measurements of Pollution in the Troposphere (MOPITT) CO retrievals with aircraft in situ profiles, J. Geophys. Res., 109, D03309~~n/a-n/a~~, http://doi.org/10.1029/2003jd004101, 2004.

Emmons, L. K., Walters, S., Hess, P. G., Lamarque, J. F., Pfister, G. G., Fillmore, D., Granier, C., Guenther, A., Kinnison, D., Laepple, T., Orlando, J., Tie, X., Tyndall, G., Wiedinmyer, C., Baughcum, S. L., and Kloster, S.: Description and evaluation of the Model for Ozone and Related chemical Tracers, version 4 (MOZART-4), Geoscientific Model Development, 3, 43-67, http://doi.org/10.5194/gmd-3-43-2010, 2010.

Evans, M. J., and Jacob, D.: Impact of new laboratory studies of N2O5hydrolysis on global model budgets of tropospheric nitrogen oxides, ozone, and OH, Geophys. Res. Lett., 32, http://doi.org/10.1029/2005gl022469, 2005.

Eyring, V., Bony, S., Meehl, G. A., Senior, C. A., Stevens, B., Stouffer, R. J., and Taylor, K. E.: Overview of the Coupled Model Intercomparison Project Phase 6 (CMIP6) experimental design and organization, Geoscientific Model Development, 9, 1937-1958, http://doi.org/10.5194/gmd-9-1937-2016, 2016.

Fairlie, T. D., Jacob, D. J., and Park, R. J.: The impact of transpacific transport of mineral dust in the United States, Atmos. Environ., 41, 1251-1266, http://doi.org/10.1016/j.atmosenv.2006.09.048, 2007.

Fiore, A. M., Naik, V., Spracklen, D. V., Steiner, A., Unger, N., Prather, M., Bergmann, D., Cameron-Smith, P. J., Cionni, I., Collins, W. J., Dalsoren, S., Eyring, V., Folberth, G. A., Ginoux, P., Horowitz, L. W., Josse, B., Lamarque, J. F., MacKenzie, I. A., Nagashima, T., O'Connor, F. M., Righi, M., Rumbold, S. T., Shindell, D. T., Skeie, R. B., Sudo, K., Szopa, S., Takemura, T., and Zeng, G.: Global air quality and climate, Chem. Soc. Rev., 41, 6663-6683, http://doi.org/10.1039/c2cs35095e, 2012.

Fischer, E. V., Jacob, D. J., Yantosca, R. M., Sulprizio, M. P., Millet, D. B., Mao, J., Paulot, F., Singh, H. B., Roiger, A., Ries, L., Talbot, R. W., Dzepina, K., and Pandey Deolal, S.: Atmospheric peroxyacetyl nitrate (PAN): a global budget and source attribution, Atmos. Chem. Phys., 14, 2679-2698, http://doi.org/10.5194/acp-14-2679-2014, 2014.

Fountoukis, C., and Nenes, A.: ISORROPIA II: a computationally efficient thermodynamic equilibrium model for K+–Ca2+–Mg2+–NH4+–Na+–SO42−–NO3−–Cl−–H2O aerosols, Atmos. Chem. Phys., 7, 4639-4659, http://doi.org/10.5194/acp-7-4639-2007, 2007.

Geddes, J. A., Heald, C. L., Silva, S. J., and Martin, R. V.: Land cover change impacts on atmospheric chemistry: simulating projected large-scale tree mortality in the United States, Atmos. Chem. Phys., 16, 2323-2340, http://doi.org/10.5194/acp-16-2323-2016, 2016.

Gong, S. L., Barrie, L. A., and Blanchet, J. P.: Modeling sea-salt aerosols in the atmosphere: 1. Model development, J. Geophys. Res., 102, 3805-3818, http://doi.org/10.1029/96jd02953, 1997.

Guenther, A. B., Jiang, X., Heald, C. L., Sakulyanontvittaya, T., Duhl, T., Emmons, L. K., and Wang, X.: The Model of Emissions of Gases and Aerosols from Nature version 2.1 (MEGAN2.1): an extended and updated framework for modeling biogenic emissions, Geoscientific Model Development, 5, 1471-1492, http://doi.org/10.5194/gmd-5-1471-2012, 2012.

Hardacre, C., Wild, O., and Emberson, L.: An evaluation of ozone dry deposition in global scale chemistry climate models, Atmos. Chem. Phys., 15, 6419-6436, http://doi.org/10.5194/acp-15-6419-2015, 2015.

Hoesly, R. M., Smith, S. J., Feng, L., Klimont, Z., Janssens-Maenhout, G., Pitkanen, T., Seibert, J. J., Vu, L., Andres, R. J., Bolt, R. M., Bond, T. C., Dawidowski, L., Kholod, N., Kurokawa, J.-i., Li, M., Liu, L., Lu, Z., Moura, M. C. P., amp, apos, Rourke, P. R., and Zhang, Q.: Historical (1750–2014) anthropogenic emissions of reactive gases and aerosols from the Community Emissions Data System (CEDS), Geoscientific Model Development, 11, 369-408, http://doi.org/10.5194/gmd-11-369-2018, 2018.

Holtslag, A. A. M. and Boville, B. A.: Local versus nonlocal boundary-layer diffusion in a global climate model, J. Climate, 6, 1825–1842, 1993.

Hu, L., Jacob, D. J., Liu, X., Zhang, Y., Zhang, L., Kim, P. S., Sulprizio, M. P., and Yantosca, R. M.: Global budget of tropospheric ozone: Evaluating recent model advances with satellite (OMI), aircraft (IAGOS), and ozonesonde observations, Atmos. Environ., 167, 323-334, http://doi.org/10.1016/j.atmosenv.2017.08.036, 2017.

Hu, L., Keller, C. A., Long, M. S., Sherwen, T., Auer, B., Da Silva, A., Nielsen, J. E., Pawson, S., Thompson, M. A., Trayanov, A. L., Travis, K. R., Grange, S. K., Evans, M. J., and Jacob, D. J.: Global simulation of tropospheric chemistry at 12.5km resolution: performance and evaluation of the GEOS-Chem chemical module (v10-1) within the NASA GEOS Earth system model (GEOS-5 ESM), Geoscientific Model Development, 11, 4603-4620, http://doi.org/10.5194/gmd-11-4603-2018, 2018.

Huang, G., Liu, X., Chance, K., Yang, K., Bhartia, P. K., Cai, Z., Allaart, M., Ancellet, G., Calpini, B., Coetzee, G. J. R., Cuevas-Agulló, E., Cupeiro, M., De Backer, H., Dubey, M. K., Fuelberg, H. E., Fujiwara, M., Godin-Beekmann, S., Hall, T. J., Johnson, B., Joseph, E., Kivi, R., Kois, B., Komala, N., König-Langlo, G., Laneve, G., Leblanc, T., Marchand, M., Minschwaner, K. R., Morris, G., Newchurch, M. J., Ogino, S.-Y., Ohkawara, N., Piters, A. J. M., Posny, F., Querel, R., Scheele, R., Schmidlin, F. J., Schnell, R. C., Schrems, O., Selkirk, H., Shiotani, M., Skrivánková, P., Stübi, R., Taha, G., Tarasick, D. W., Thompson, A. M., Thouret, V., Tully, M. B., Van Malderen, R., Vömel, H., von der Gathen, P., Witte, J. C., and Yela, M.: Validation of 10-year SAO OMI Ozone Profile (PROFOZ) product using ozonesonde observations, Atmospheric Measurement Techniques, 10, 2455-2475, http://doi.org/10.5194/amt-10-2455-2017, 2017.

Huang, G., Liu, X., Chance, K., Yang, K., and Cai, Z.: Validation of 10-year SAO OMI ozone profile (PROFOZ) product using Aura MLS measurements, Atmospheric Measurement Techniques, 11, 17-32, http://doi.org/10.5194/amt-11-17-2018, 2018.

IPCC: Climate Change 2013: The Physical Science Basis. Contribution of Working Group I to the Fifth Assessment Report of the Intergovernmental Panel on Climate Change [Stocker, T.F., D. Qin, G.-K. Plattner, M. Tignor, S.K. Allen, J. Boschung, A. Nauels, Y. Xia, V. Bex and P.M. Midgley (eds.)], Cambridge University Press, Cambridge, United Kingdom and New York, NY, USA, 1535 pp, http://doi.org/10.1017/CBO9781107415324, 2013.

Jacob, D.: Heterogeneous chemistry and tropospheric ozone, Atmos. Environ., 34, 2131-2159, http://doi.org/10.1016/s1352-2310(99)00462-8, 2000.

Jacob, D. J., and Winner, D. A.: Effect of climate change on air quality, Atmos. Environ., 43, 51-63, http://doi.org/10.1016/j.atmosenv.2008.09.051, 2009.

Jaeglé, L., Quinn, P. K., Bates, T. S., Alexander, B., and Lin, J. T.: Global distribution of sea salt aerosols: new constraints from in situ and remote sensing observations, Atmos. Chem. Phys., 11, 3137-3157, http://doi.org/10.5194/acp-11-3137-2011, 2011.

Ji, J.: A Climate-Vegetation Interaction Model: Simulating Physical and Biological Processes at the Surface, J. Biogeogr., 22, 445, http://doi.org/10.2307/2845941, 1995.

Ji, J., Huang, M., and Li, K.: Prediction of carbon exchanges between China terrestrial ecosystem and atmosphere in 21st century, Science in China Series D: Earth Sciences, 51, 885-898, http://doi.org/10.1007/s11430-008-0039-y, 2008.

Keller, C. A., Long, M. S., Yantosca, R. M., Da Silva, A. M., Pawson, S., and Jacob, D. J.: HEMCO v1.0: a versatile, ESMF compliant component for calculating emissions in atmospheric models, Geosci. Model Dev., 7, 1409–1417, doi:10.5194/gmd-7-1409-2014, 2014.

Kodros, J. K., Pierce, J. R.: Important global and regional differences in cloud-albedo aerosol indirect effect estimates between simulations with and without prognostic aerosol microphysics, J. Geophys. Res., 122, doi:10.1002/2016JD025886, 2017.

Krotkov, N. A.: OMI/Aura NO2 Cloud-Screened Total and Tropospheric Column L3 Global Gridded 0.25 degree x 0.25 degree V3, 2013.

Krotkov, N. A.: OMI/Aura Sulfur Dioxide (SO_2) Total Column L3 1 day Best Pixel in 0.25 degree x 0.25 degree V3, http://doi.org/10.5067/Aura/OMI/DATA3008, 2015.

Lamarque, J. F., Bond, T. C., Eyring, V., Granier, C., Heil, A., Klimont, Z., Lee, D., Liousse, C., Mieville, A., Owen, B., Schultz, M. G., Shindell, D., Smith, S. J., Stehfest, E., Van Aardenne, J., Cooper, O. R., Kainuma, M., Mahowald, N., McConnell, J. R., Naik, V., Riahi, K., and van Vuuren, D. P.: Historical (1850–2000) gridded anthropogenic and biomass burning emissions of reactive gases and aerosols: methodology and application, Atmos. Chem. Phys., 10, 7017-7039, http://doi.org/10.5194/acp-10-7017-2010, 2010.

Lamarque, J.-F., Emmons, L. K., Hess, P. G., Kinnison, D. E., Tilmes, S., Vitt, F., Heald, C. L., Holland, E. A., Lauritzen, P. H., Neu, J., Orlando, J. J., Rasch, P. J., and Tyndall, G. K.: CAM-chem: description and evaluation of interactive atmospheric chemistry in the Community Earth System Model, Geosci. Model Dev., 5, 369-411, https://doi.org/10.5194/gmd-5-369-2012, 2012.

Lee, C., Martin, R. V., van Donkelaar, A., O'Byrne, G., Krotkov, N., Richter, A., Huey, L. G., and Holloway, J. S.: Retrieval of vertical columns of sulfur dioxide from SCIAMACHY and OMI: Air mass factor algorithm development, validation, and error analysis, J. Geophys. Res., 114, http://doi.org/10.1029/2009jd012123, 2009.

Li, W., Y., Zhang, X., Shi, W., Zhou, A. Huang, M. Mu, J. Ji.: Development of Land Surface Model BCC_AVIM2.0 and its Preliminary Performances in LS3MIP/CMIP6, J. Meteoro. Res., 33, 2019, in press.

Lin, H., Feng, X., Fu, T.-M., Tian, H., Ma, Y., Zhang, L., Jacob, D. J., Yantosca, R. M., Sulprizio, M. P., Lundgren, E. W., Zhuang, J., Zhang, Q., Lu, X., Zhang, L., Shen, L., Guo, J., Eastham, S. D., and Keller, C. A.: WRF-GC: online coupling of WRF and GEOS-Chem for regional atmospheric chemistry modeling, Part 1: description of the one-way model (v1.0), Geosci. Model Dev. Discuss., http://doi.org/10.5194/gmd-2019-333, 2020.

Liu, H., Jacob, D. J., Bey, I., and Yantosca, R. M.: Constraints from210Pb and7Be on wet deposition and transport in a global three-dimensional chemical tracer model driven by assimilated meteorological fields, J. Geophys. Res., 106, 12109-12128, http://doi.org/10.1029/2000jd900839, 2001.

Liu, X., Chance, K., Sioris, C. E., Spurr, R. J. D., Kurosu, T. P., Martin, R. V., and Newchurch, M. J.: Ozone profile and tropospheric ozone retrievals from the Global Ozone Monitoring Experiment: Algorithm description and validation, J. Geophys. Res., 110, http://doi.org/10.1029/2005jd006240, 2005.

Liu, X., Bhartia, P. K., Chance, K., Spurr, R. J. D., and Kurosu, T. P.: Ozone profile retrievals from the Ozone Monitoring Instrument, Atmos. Chem. Phys., 10, 2521-2537, http://doi.org/10.5194/acp-10-2521-2010, 2010.

Long, M. S., Yantosca, R., Nielsen, J. E., Keller, C. A., da Silva, A., Sulprizio, M. P., Pawson, S., and Jacob, D. J.: Development of a grid-independent GEOS-Chem chemical transport model (v9-02) as an atmospheric chemistry module for Earth system models, Geoscientific Model Development, 8, 595-602, http://doi.org/10.5194/gmd-8-595-2015, 2015.

Lu, X., Zhang, L., Liu, X., Gao, M., Zhao, Y., and Shao, J.: Lower tropospheric ozone over India and its linkage to the South Asian monsoon, Atmos. Chem. Phys., 18, 3101-3118, http://doi.org/10.5194/acp-18-3101-2018, 2018.

Lu, X., Zhang, L., and Shen, L.: Meteorology and Climate Influences on Tropospheric Ozone: a Review of Natural Sources, Chemistry, and Transport Patterns, Current Pollution Reports, 5, 238-260, http://doi.org/10.1007/s40726-019-00118-3, 2019a.

Lu, X., Zhang, L., Zhao, Y., Jacob, D. J., Hu, Y., Hu, L., Gao, M., Liu, X., Petropavlovskikh, I., McClure-Begley, A., and Querel, R.: Surface and tropospheric ozone trends in the Southern Hemisphere since 1990: possible linkages to poleward expansion of the Hadley circulation, Science Bulletin, 64, 400-409, http://doi.org/10.1016/j.scib.2018.12.021, 2019b.

Mao, J., Jacob, D. J., Evans, M. J., Olson, J. R., Ren, X., Brune, W. H., Clair, J. M. S., Crounse, J. D., Spencer, K. M., Beaver, M. R., Wennberg, P. O., Cubison, M. J., Jimenez, J. L., Fried, A., Weibring, P., Walega, J. G., Hall, S. R., Weinheimer, A. J., Cohen, R. C., Chen, G., Crawford, J. H., McNaughton, C., Clarke, A. D., Jaeglé, L., Fisher, J. A., Yantosca, R. M., Le Sager, P., and Carouge, C.: Chemistry of hydrogen oxide radicals (HO_x) in the Arctic troposphere in spring, Atmos. Chem. Phys., 10, 5823-5838, http://doi.org/10.5194/acp-10-5823-2010, 2010.

Mao, J., Paulot, F., Jacob, D. J., Cohen, R. C., Crounse, J. D., Wennberg, P. O., Keller, C. A., Hudman, R. C., Barkley, M. P., and Horowitz, L. W.: Ozone and organic nitrates over the eastern United States: Sensitivity to isoprene chemistry, J. Geophys. Res., 118, 11,256-211,268, http://doi.org/10.1002/jgrd.50817, 2013.

Marais, E. A., Jacob, D. J., Jimenez, J. L., Campuzano-Jost, P., Day, D. A., Hu, W., Krechmer, J., Zhu, L., Kim, P. S., Miller, C. C., Fisher, J. A., Travis, K., Yu, K., Hanisco, T. F., Wolfe, G. M., Arkinson, H. L., Pye, H. O. T., Froyd, K. D., Liao, J., and McNeill, V. F.: Aqueous-phase mechanism for secondary organic aerosol formation from isoprene: application to the southeast United States and co-benefit of SO2 emission controls, Atmos. Chem. Phys., 16, 1603-1618, http://doi.org/10.5194/acp-16-1603-2016, 2016.

Martin, R. V., Jacob, D. J., Yantosca, R. M., Chin, M., and Ginoux, P.: Global and regional decreases in tropospheric oxidants from photochemical effects of aerosols, J. Geophys. Res., 108, n/a-n/a, http://doi.org/10.1029/2002jd002622, 2003.

McLinden, C. A., Olsen, S. C., Hannegan, B., Wild, O., Prather, M. J., and Sundet, J.: Stratospheric ozone in 3-D models: A simple chemistry and the cross-tropopause flux, J. Geophys. Res., 105, 14653-14665, http://doi.org/10.1029/2000jd900124, 2000.

Meinshausen, M., Vogel, E., Nauels, A., Lorbacher, K., Meinshausen, N., Etheridge, D. M., Fraser, P. J., Montzka, S. A., Rayner, P. J., Trudinger, C. M., Krummel, P. B., Beyerle, U., Canadell, J. G., Daniel, J. S., Enting, I. G., Law, R. M., Lunder, C. R., amp, apos, Doherty, S., Prinn, R. G., Reimann, S., Rubino, M., Velders, G. J. M., Vollmer, M. K., Wang, R. H. J., and Weiss, R.: Historical greenhouse gas concentrations for climate modelling (CMIP6), Geoscientific Model Development, 10, 2057-2116, http://doi.org/10.5194/gmd-10-2057-2017, 2017._

Millet, D. B., Guenther, A., Siegel, D. A., Nelson, N. B., Singh, H. B., de Gouw, J. A., Warneke, C., Williams, J., Eerdekens, G., Sinha, V., Karl, T., Flocke, F., Apel, E., Riemer, D. D., Palmer, P. I., and Barkley, M.: Global atmospheric budget of acetaldehyde: 3-D model analysis and constraints from in-situ and satellite observations, Atmos. Chem. Phys., 10, 3405-3425, http://doi.org/10.5194/acp-10-3405-2010, 2010.

Monahan, E. C., Spiel, D. E., and Davidso, K. L.: A model of marine aerosol generation via whitecaps and wave disruption, in Oceanic Whitecaps, edited by E. C. Monahan and G. Mac Niocail, 1986.

Naik, V., Voulgarakis, A., Fiore, A. M., Horowitz, L. W., Lamarque, J. F., Lin, M., Prather, M. J., Young, P. J., Bergmann, D., Cameron-Smith, P. J., Cionni, I., Collins, W. J., Dalsøren, S. B., Doherty, R., Eyring, V., Faluvegi, G., Folberth, G. A., Josse, B., Lee, Y. H., MacKenzie, I. A., Nagashima, T., van Noije, T. P. C., Plummer, D. A., Righi, M., Rumbold, S. T., Skeie, R., Shindell, D. T., Stevenson, D. S., Strode, S., Sudo, K., Szopa, S., and Zeng, G.: Preindustrial to present-day changes in tropospheric hydroxyl radical and methane lifetime from the Atmospheric Chemistry and Climate Model Intercomparison Project (ACCMIP), Atmos. Chem. Phys., 13, 5277-5298, http://doi.org/10.5194/acp-13-5277-2013, 2013._

Nicely, J. M., Duncan, B. N., Hanisco, T. F., Wolfe, G. M., Salawitch, R. J., Deushi, M., Haslerud, A. S., Jöckel, P., Josse, B., Kinnison, D. E., Klekociuk, A., Manyin, M. E., Marécal, V., Morgenstern, O., Murray, L. T., Myhre, G., Oman, L. D., Pitari, G., Pozzer, A., Quaglia, I., Revell, L. E., Rozanov, E., Stenke, A., Stone, K., Strahan, S., Tilmes, S., Tost, H., Westervelt, D. M., and Zeng, G.: A machine learning examination of hydroxyl radical differences among model simulations for CCMI-1, Atmos. Chem. Phys., 20, 1341-1361, http://doi.org/10.5194/acp-20-1341-2020, 2020.

Ott, L. E., Pickering, K. E., Stenchikov, G. L., Allen, D. J., DeCaria, A. J., Ridley, B., Lin, R.-F., Lang, S., and Tao, W.-K.: Production of lightning NOxand its vertical distribution calculated from three-dimensional cloud-scale chemical transport model simulations, J. Geophys. Res., 115, http://doi.org/10.1029/2009jd011880, 2010.

Park, R. J., Jacob, D. J., Field, B. D., Yantosca, R. M., and Chin, M.: Natural and transboundary pollution influences on sulfate-nitrate-ammonium aerosols in the United States: Implications for policy, J Geophys Res-Atmos, 109, http://doi.org/10.1029/2003jd004473, 2004.

Parrella, J. P., Jacob, D. J., Liang, Q., Zhang, Y., Mickley, L. J., Miller, B., Evans, M. J., Yang, X., Pyle, J. A., Theys, N., and Van Roozendael, M.: Tropospheric bromine chemistry: implications for present and pre-industrial ozone and mercury, Atmos. Chem. Phys., 12, 6723-6740, http://doi.org/10.5194/acp-12-6723-2012, 2012._

Pfister, G., Hess, P. G., Emmons, L. K., Lamarque, J. F., Wiedinmyer, C., Edwards, D. P., Petron, G., Gille, J. C., and Sachse, G. W.: Quantifying CO emissions from the 2004 Alaskan wildfires using MOPITT CO data, Geophys. Res. Lett., 32, http://doi.org/Artn L1180910.1029/2005gl022995, 2005.

Price, C., and Rind, D.: A simple lightning parameterization for calculating global lightning distributions, J. Geophys. Res., 97, 9919-9933, http://doi.org/10.1029/92jd00719, 1992.

Price, C., Penner, J., and Prather, M.: NOxfrom lightning: 1. Global distribution based on lightning physics, J. Geophys. Res., 102, 5929-5941, http://doi.org/10.1029/96jd03504, 1997.

Pye, H. O. T., Liao, H., Wu, S., Mickley, L. J., Jacob, D. J., Henze, D. K., and Seinfeld, J. H.: Effect of changes in climate and emissions on future sulfate-nitrate-ammonium aerosol levels in the United States, J. Geophys. Res., 114, http://doi.org/10.1029/2008jd010701, 2009.

Rodgers, C. D.: Inverse Methods for Atmospheric Sounding: Theory and Practice, 2000.

Sauvage, B., R. V. Martin, A. van Donkelaar, and J. R. Ziemke (2007), Quantification of the factors controlling tropical tropospheric ozone and the South Atlantic maximum, J. Geophys. Res., 112, D11309, doi:10.1029/2006JD008008.

Schultz, M. G., Schröder, S., Lyapina, O., Cooper, O., Galbally, I., Petropavlovskikh, I., Von Schneidemesser, E., Tanimoto, H., Elshorbany, Y., Naja, M., Seguel, R., Dauert, U., Eckhardt, P., Feigenspahn, S., Fiebig, M., Hjellbrekke, A.-G., Hong, Y.-D., Christian Kjeld, P., Koide, H., Lear, G., Tarasick, D., Ueno, M., Wallasch, M., Baumgardner, D., Chuang, M.-T., Gillett, R., Lee, M., Molloy, S., Moolla, R., Wang, T., Sharps, K., Adame, J. A., Ancellet, G., Apadula, F., Artaxo, P., Barlasina, M., Bogucka, M., Bonasoni, P., Chang, L., Colomb, A., Cuevas, E., Cupeiro, M., Degorska, A., Ding, A., Fröhlich, M., Frolova, M., Gadhavi, H., Gheusi, F., Gilge, S., Gonzalez, M. Y., Gros, V., Hamad, S. H., Helmig, D., Henriques, D., Hermansen, O., Holla, R., Huber, J., Im, U., Jaffe, D. A., Komala, N., Kubistin, D., Lam, K.-S., Laurila, T., Lee, H., Levy, I., Mazzoleni, C., Mazzoleni, L., McClure-Begley, A., Mohamad, M., Murovic, M., Navarro-Comas, M., Nicodim, F., Parrish, D., Read, K. A., Reid, N., Ries, L., Saxena, P., Schwab, J. J., Scorgie, Y., Senik, I., Simmonds, P., Sinha, V., Skorokhod, A., Spain, G., Spangl, W., Spoor, R., Springston, S. R., Steer, K., Steinbacher, M., Suharguniyawan, E., Torre, P., Trickl, T., Weili, L., Weller, R., Xu, X., Xue, L., and Zhiqiang, M.: Tropospheric Ozone Assessment Report, links to Global surface ozone datasets. PANGAEA, https://doi.org/10.1594/PANGAEA.876108, 2017a.

Schultz, M. G., Schröder, S., Lyapina, O., Cooper, O., Galbally, I., Petropavlovskikh, I., Von Schneidemesser, E., Tanimoto, H., Elshorbany, Y., Naja, M., Seguel, R., Dauert, U., Eckhardt, P., Feigenspahn, S., Fiebig, M., Hjellbrekke, A.-G., Hong, Y.-D., Christian Kjeld, P., Koide, H., Lear, G., Tarasick, D., Ueno, M., Wallasch, M., Baumgardner, D., Chuang, M.-T., Gillett, R., Lee, M., Molloy, S., Moolla, R., Wang, T., Sharps, K., Adame, J. A., Ancellet, G., Apadula, F., Artaxo, P., Barlasina, M., Bogucka, M., Bonasoni, P., Chang, L., Colomb, A., Cuevas, E., Cupeiro, M., Degorska, A., Ding, A., Fröhlich, M., Frolova, M., Gadhavi, H., Gheusi, F., Gilge, S., Gonzalez, M. Y., Gros, V., Hamad, S. H., Helmig, D., Henriques, D., Hermansen, O., Holla, R., Huber, J., Im, U., Jaffe, D. A., Komala, N., Kubistin, D., Lam, K.-S., Laurila, T., Lee, H., Levy, I., Mazzoleni, C., Mazzoleni, L., McClure-Begley, A., Mohamad, M., Murovic, M., Navarro-Comas, M., Nicodim, F., Parrish, D., Read, K. A., Reid, N., Ries, L., Saxena, P., Schwab, J. J., Scorgie, Y., Senik, I., Simmonds, P., Sinha, V., Skorokhod, A., Spain, G., Spangl, W., Spoor, R., Springston, S. R., Steer, K., Steinbacher, M., Suharguniyawan, E., Torre, P., Trickl, T., Weili, L., Weller, R., Xu, X., Xue, L., and Zhiqiang, M.: Tropospheric Ozone Assessment Report: Database and Metrics Data of Global Surface Ozone Observations, Elem Sci Anth, 5, 58, http://doi.org/10.1525/elementa.244, 2017b.

Schumann, U., and Huntrieser, H.: The global lightning-induced nitrogen oxides source, Atmos. Chem. Phys., 7, 3823-3907, http://doi.org/10.5194/acp-7-3823-2007, 2007.

Spivakovsky, C. M., Logan, J. A., Montzka, S. A., Balkanski, Y. J., Foreman-Fowler, M., Jones, D. B. A., Horowitz, L. W., Fusco, A. C., Brenninkmeijer, C. A. M., Prather, M. J., Wofsy, S. C., and McElroy, M. B.: Three-dimensional climatological distribution of tropospheric OH: Update and evaluation, J. Geophys. Res., 105, 8931-8980, http://doi.org/10.1029/1999jd901006, 2000.

Stevens, B., Fiedler, S., Kinne, S., Peters, K., Rast, S., Müsse, J., Smith, S. J., and Mauritsen, T.: MACv2-SP: a parameterization of anthropogenic aerosol optical properties and an associated Twomey effect for use in CMIP6, Geosci. Model Dev., 10, 433–452, https://doi.org/10.5194/gmd-10-433-2017, 2017.

Thompson, A. M.: Southern Hemisphere Additional Ozonesondes (SHADOZ) 1998–2000 tropical ozone climatology 1. Comparison with Total Ozone Mapping Spectrometer (TOMS) and ground-based measurements, J. Geophys. Res., 108, http://doi.org/10.1029/2001jd000967, 2003.

Tilmes, S., Lamarque, J. F., Emmons, L. K., Conley, A., Schultz, M. G., Saunois, M., Thouret, V., Thompson, A. M., Oltmans, S. J., Johnson, B., and Tarasick, D.: Technical Note: Ozonesonde climatology between 1995 and 2011: description, evaluation and applications, Atmos. Chem. Phys., 12, 7475-7497, http://doi.org/10.5194/acp-12-7475-2012, 2012.

van Marle, M. J. E., Kloster, S., Magi, B. I., Marlon, J. R., Daniau, A.-L., Field, R. D., Arneth, A., Forrest, M., Hantson, S., Kehrwald, N. M., Knorr, W., Lasslop, G., Li, F., Mangeon, S., Yue, C., Kaiser, J. W., and van der Werf, G. R.: Historic global biomass burning emissions for CMIP6 (BB4CMIP) based on merging satellite observations with proxies and fire models (1750–2015), Geoscientific Model Development, 10, 3329-3357, http://doi.org/10.5194/gmd-10-3329-2017, 2017.

Wang, S., Hornbrook, R. S., Hills, A., Emmons, L. K., Tilmes, S., Lamarque, J. F., Jimenez, J. L., Campuzano-Jost, P., Nault, B. A., Crounse, J. D., Wennberg, P. O., Kim, M., Allen, H., Ryerson, T. B., Thompson, C. R., Peischl, J., Moore, F., Nance, D., Hall, B., Elkins, J., Tanner, D., Huey, L. G., Hall, S. R., Ullmann, K., Orlando, J. J., Tyndall, G. S., Flocke, F. M., Ray, E., Hanisco, T. F., Wolfe, G. M., St. Clair, J., Commane, R., Daube, B., Barletta, B., Blake, D. R., Weinzierl, B., Dollner, M., Conley, A., Vitt, F., Wofsy, S. C., Riemer, D. D., and Apel, E. C.: Atmospheric Acetaldehyde: Importance of Air-Sea Exchange and a Missing Source in the Remote Troposphere, Geophys. Res. Lett., 46, 5601-5613, http://doi.org/10.1029/2019gl082034, 2019.

Wesely, M. L.: Parameterization of Surface Resistances to Gaseous Dry Deposition in Regional-Scale Numerical-Models, Atmos. Environ., 23, 1293-1304, http://doi.org/Doi 10.1016/0004-6981(89)90153-4, 1989.

Wild, O., and Prather, M. J.: Global tropospheric ozone modeling: Quantifying errors due to grid resolution, J. Geophys. Res., 111, http://doi.org/10.1029/2005jd006605, 2006.

Williamson, D. L., and P. J. Rasch, Two-dimensional semi-Lagrangian transport with shapepreserving interpolation, Mon. Wea. Rev., 117, 102–129, 1989.

Wu, T., Yu, R., and Zhang, F.: A Modified Dynamic Framework for the Atmospheric Spectral Model and Its Application, J Atmos Sci, 65, 2235-2253, http://doi.org/10.1175/2007jas2514.1, 2008.

Wu, T., Yu, R., Zhang, F., Wang, Z., Dong, M., Wang, L., Jin, X., Chen, D., and Li, L.: The Beijing Climate Center atmospheric general circulation model: description and its performance for the present-day climate, Climate Dynamics, 34, 123-147, http://doi.org/10.1007/s00382-008-0487-2, 2010.

Wu, T.: A mass-flux cumulus parameterization scheme for large-scale models: description and test with observations, Climate Dynamics, 38, 725-744, http://doi.org/10.1007/s00382-011-0995-3, 2012.

Wu, T., Li, W., Ji, J., Xin, X., Li, L., Wang, Z., Zhang, Y., Li, J., Zhang, F., Wei, M., Shi, X., Wu, F., Zhang, L., Chu, M., Jie, W., Liu, Y., Wang, F., Liu, X., Li, Q., Dong, M., Liang, X., Gao, Y., and Zhang, J.: Global carbon budgets simulated by the Beijing Climate Center Climate System Model for the last century, J. Geophys. Res., 118, 4326-4347, http://doi.org/10.1002/jgrd.50320, 2013.

Wu, T., Song, L., Li, W., Wang, Z., Zhang, H., Xin, X., Zhang, Y., Zhang, L., Li, J., Wu, F., Liu, Y., Zhang, F., Shi, X., Chu, M., Zhang, J., Fang, Y., Wang, F., Lu, Y., Liu, X., Wei, M., Liu, Q., Zhou, W., Dong, M., Zhao, Q., Ji, J., Li, L., and Zhou, M.: An overview of BCC climate system model development and application for climate change studies, Acta Meteorologica Sinica, 28, 34-56, http://doi.org/10.1007/s13351-014-3041-7, 2014.

Wu, T., Lu, Y., Fang, Y., Xin, X., Li, L., Li, W., Jie, W., Zhang, J., Liu, Y., Zhang, L., Zhang, F., Zhang, Y., Wu, F., Li, J., Chu, M., Wang, Z., Shi, X., Liu, X., Wei, M., Huang, A., Zhang, Y., and Liu, X.: The Beijing Climate Center Climate System Model (BCC-CSM): the main progress from CMIP5 to CMIP6, Geoscientific Model Development, 12, 1573-1600, http://doi.org/10.5194/gmd-12-1573-2019, 2019.

Wu, T., Zhang, F., Zhang, J., Jie, W., Zhang, Y., Wu, F., Li, L., Yan, J., Liu, X., Lu, X., Tan, H., Zhang, L., Wang, J., and Hu, A.: Beijing Climate Center Earth System Model version 1 (BCC-ESM1): model description and evaluation of aerosol simulations, Geoscientific Model Development, 13, 977-1005, http://doi.org/10.5194/gmd-13-977-2020, 2020.

Xin, X., T. Wu, and J. Zhang, 2013: Introduction of CMIP5 experiments carried out with the climate system models of Beijing Climate Center. Adv. Clim. Change Res., 4(1), 41-49，doi: 10.3724/SP.J.1248.2013.041.

Young, P. J., Archibald, A. T., Bowman, K. W., Lamarque, J. F., Naik, V., Stevenson, D. S., Tilmes, S., Voulgarakis, A., Wild, O., Bergmann, D., Cameron-Smith, P., Cionni, I., Collins, W. J., Dalsøren, S. B., Doherty, R. M., Eyring, V., Faluvegi, G., Horowitz, L. W., Josse, B., Lee, Y. H., MacKenzie, I. A., Nagashima, T., Plummer, D. A., Righi, M., Rumbold, S. T., Skeie, R. B., Shindell, D. T., Strode, S. A., Sudo, K., Szopa, S., and Zeng, G.: Pre-industrial to end 21st century projections of tropospheric ozone from the Atmospheric Chemistry and Climate Model Intercomparison Project (ACCMIP), Atmos. Chem. Phys., 13, 2063-2090, http://doi.org/10.5194/acp-13-2063-2013, 2013.

Young, P. J., Naik, V., Fiore, A. M., Gaudel, A., Guo, J., Lin, M. Y., Neu, J. L., Parrish, D. D., Rieder, H. E., Schnell, J. L., Tilmes, S., Wild, O., Zhang, L., Ziemke, J. R., Brandt, J., Delcloo, A., Doherty, R. M., Geels, C., Hegglin, M. I., Hu, L., Im, U., Kumar, R., Luhar, A., Murray, L., Plummer, D., Rodriguez, J., Saiz-Lopez, A., Schultz, M. G., Woodhouse, M. T., and Zeng, G.: Tropospheric Ozone Assessment Report: Assessment of global-scale model performance for global and regional ozone distributions, variability, and trends, Elem Sci Anth, 6, 10, http://doi.org/10.1525/elementa.265, 2018.

Yu, F., and G. Luo, Simulation of particle size distribution with a global aerosol model: Contribution of nucleation to aerosol and CCN number concentrations, Atmos. Chem. Phys., 9, 7691-7710, https://doi.org/10.5194/acp-9-7691-2009, 2009.

Yu, K., Jacob, D. J., Fisher, J. A., Kim, P. S., Marais, E. A., Miller, C. C., Travis, K. R., Zhu, L., Yantosca, R. M., Sulprizio, M. P., Cohen, R. C., Dibb, J. E., Fried, A., Mikoviny, T., Ryerson, T. B., Wennberg, P. O., and Wisthaler, A.: Sensitivity to grid resolution in the ability of a chemical transport model to simulate observed oxidant chemistry under high-isoprene conditions, Atmos. Chem. Phys., 16, 4369-4378, http://doi.org/10.5194/acp-16-4369-2016, 2016.

Zender, C. S.: Mineral Dust Entrainment and Deposition (DEAD) model: Description and 1990s dust climatology, J. Geophys. Res., 108, http://doi.org/10.1029/2002jd002775, 2003.

Zhang, L., Jacob, D. J., Liu, X., Logan, J. A., Chance, K., Eldering, A., and Bojkov, B. R.: Intercomparison methods for satellite measurements of atmospheric composition: application to tropospheric ozone from TES and OMI, Atmos. Chem. Phys., 10, 4725-4739, http://doi.org/10.5194/acp-10-4725-2010, 2010.

Zhang, L., Jacob, D. J., Knipping, E. M., Kumar, N., Munger, J. W., Carouge, C. C., van Donkelaar, A., Wang, Y. X., and Chen, D.: Nitrogen deposition to the United States: distribution, sources, and processes, Atmos. Chem. Phys., 12, 4539–4554, http://10.5194/acp-12-4539-2012, 2012.

Zhang, L. M., Gong, S. L., Padro, J., and Barrie, L.: A size-segregated particle dry deposition scheme for an atmospheric aerosol module, Atmos. Environ., 35, 549-560, http://doi.org/Doi 10.1016/S1352-2310(00)00326-5, 2001.

Zhang, Y., Cooper, O. R., Gaudel, A., Thompson, A. M., Nédélec, P., Ogino, S.-Y., and West, J. J.: Tropospheric ozone change from 1980 to 2010 dominated by equatorward redistribution of emissions, Nature Geosci., 9, 875-879, 10.1038/ngeo2827, 2016.

Zhao, S., and He, W.: Evaluation of the performance of the Beijing Climate Centre Climate System Model 1.1(m) to simulate precipitation across China based on long-range correlation characteristics, J. Geophys. Res., 120, 12576-12588, http://doi.org/10.1002/2015jd024059, 2015.

Zhao, Y., Zhang, L., Tai, A. P. K., Chen, Y., and Pan, Y.: Responses of surface ozone air quality to anthropogenic nitrogen deposition in the Northern Hemisphere, Atmos. Chem. Phys., 17, 9781-9796, http://doi.org/10.5194/acp-17-9781-2017, 2017

Zhu, L., Jacob, D. J., Kim, P. S., Fisher, J. A., Yu, K., Travis, K. R., Mickley, L. J., Yantosca, R. M., Sulprizio, M. P., De Smedt, I., Abad, G. G., Chance, K., Li, C., Ferrare, R., Fried, A., Hair, J. W., Hanisco, T. F., Richter, D., Scarino, A. J., Walega, J., Weibring, P., and Wolfe, G. M.: Observing atmospheric formaldehyde (HCHO) from space: validation and intercomparison of six retrievals from four satellites (OMI, GOME2A, GOME2B, OMPS) with SEAC(4)RS aircraft observations over the Southeast US, Atmos. Chem. Phys., 16, 13477-13490, http://doi.org/10.5194/acp-16-13477-2016, 2016.

Zhu, L., González Abad, G., Nowlan, C. R., Chan Miller, C., Chance, K., Apel, E. C., DiGangi, J. P., Fried, A., Hanisco, T. F., Hornbrook, R. S., Hu, L., Kaiser, J., Keutsch, F. N., Permar, W., St. Clair, J. M., and Wolfe, G. M.: Validation of satellite formaldehyde (HCHO) retrievals using observations from 12 aircraft campaigns, Atmospheric Chemistry and Physics Discussions, http://doi.org/10.5194/acp-2019-1117, 2020.

Zhuang, J., Jacob, D. J., Gaya, J. F., Yantosca, R. M., Lundgren, E. W., Sulprizio, M. P., and Eastham, S. D.: Enabling immediate access to Earth science models through cloud computing: application to the GEOS-Chem model, Bulletin of the American Meteorological Society, http://doi.org/10.1175/bams-d-18-0243.1, 2019.

Table 1. Mapping of land use types (LUT) used in BCC-GEOS-Chem v1.0 to the Wesely deposition surfaces for deposition. Also shown are the roughness heights (Z_o) for each LUT.

	BCC-AVIM LUT	GEOS-Chem LUT for dry deposition	Z_o (m)
0	bareground	desert	0.001
1	needleleaf evergreen temperate tree	coniferous forest	1
2	needleleaf evergreen boreal tree	coniferous forest	1
3	needleleaf deciduous boreal tree	coniferous forest	1
4	broadleaf evergreen tropical tree	Amazon forest	1
5	broadleaf evergreen temperate tree	deciduous forest	1
6	broadleaf deciduous tropical tree	deciduous forest	1
7	broadleaf deciduous temperate tree	deciduous forest	1
8	broadleaf deciduous boreal tree	deciduous forest	1
9	broadleaf evergreen shrub	shrub/grassland	0.01
10	broadleaf deciduous temperate shrub	shrub/grassland	0.01
11	broadleaf deciduous boreal shrub	shrub/grassland	0.01
12	C3 arctic grass	tundra	0.002
13	C3 non-arctic grass	tundra	0.01
14	C4 grass	tundra	0.01
15	crop	agricultural land	0.1
16	wheat	agricultural land	0.1
17	ocean	water	0.001
18	glacier	snow/ice	0.0001
19	lake	water	0.001
20	wetland	wetland	0.05
21	urban	urban	2.5

Table 2. Global annual emissions used in the BCC-GEOS-Chem v1.0 categorized by sectors in unit of Tg year^{-1}

Species	Anthropogenic	Biomass burning	Biogenic	Ocean	Soil	Aircraft	Others	Total
NO	91.5	6.4			11.2	2.0	Lightning: 11.5	122.6
CO	617.2	231.8	75.9			0.6		925.5
ALK4(C_4H_{10})	17.7	0.2	26.1					44.0
ALK5(C_5H_{12})	21.4							21.4
ALK6(C_6H_{14})	26.5							26.5
Acetone (CH_3COCH_3)	1.1	3.1	19.2	9.9				33.3
ALD2(CH_3CHO)	1.2	2.4						3.6
ISOP			410.0					410.0
C_2H_4	5.9	3.2	7.5					16.6
C_3H_6 (PRPE)	3.6	2.5	10.7					16.8
C_3H_8	6.7	0.5						7.2
CH_2O	2.5	3.2						5.7
C_2H_6	6.6	2.7						9.3
BENZ(C_6H_6)	6.7							6.7
TOLU(C_7H_8)	7.8							7.8
XYLE(C_8H_{10})	7.5							7.5
SO_2	112.5	1.7				0.3	Volcano: 9.2	123.7
NH_3	60.1	2.9		8.2	2.4			73.6
DMS				27.4				27.6
BC	7.9	1.3				<0.1		9.2
OC	19.5	11.5				<0.1		31.0

Table 3. Observational datasets used for model evaluation

Species	**Observation**	**Horizontal Resolution**	**Vertical Levels**	**Data sources or reference**
Ozone	WOUDC network		Vertical profile	http://woudc.org/data.php (last access: 2 June 2019)
	TOAR dataset		Surface	Schultz et al. (2017a, https://doi.org/10.1594/PANGAEA.876108, last access: 2 June 2019)
	OMI satellite (Level 2)	2°×2.5°	24 layers	Liu et al. (2010)
CO	MOPITT satellite (Level 3)	1°×1°	~~Total column~~700 hPa	https://www2.acom.ucar.edu/mopitt (last access: 17 June 2020) (Deeter et al., 2017)
NO_2	OMI satellite (Level 3)	0.25°×0.25°	Tropospheric column	https://disc.gsfc.nasa.gov/datasets/OMNO2d_003/summary (last access: 2 June 2019) (Krotkov, 2013)
CH_2O	OMI satellite (Level 3)	0.25°×0.25°	Tropospheric column	http://h2co.aeronomie.be/ (last access: 2 June 2019) (De Smedt et al., 2015)
SO_2	OMI satellite (Level 3)	0.25°×0.25°	Tropospheric column	https://disc.gsfc.nasa.gov/datasets/OMSO2e_003/summary (last access: 2 June 2019) (Krotkov et al., 2015)
AOD	MODIS	1°×1°	Atmosphere	(https://neo.sci.gsfc.nasa.gov/view.php?datasetId=MODAL2_M_AER_OD, last access: 2 June 2019)
Aerosol composition	IMPROVE network		Surface	Interagency Monitoring of Protected Visual Environments (IMPROVE) (http://vista.cira.colostate.edu/Improve/, last access: 7 July 2019)

Table 4. Global budget of tropospheric ozone diagnosed in BCC-GEOS-Chem v1.0 and comparison with other studies.

Diagnostic term	BCC-GEOS-Chem (this study)	Classic GEOS-Chem (Hu et al., 2017)[a]	Other references
Ozone burden (Tg)	336	351	mean: 340, range: 250-410[b]
O_x chemical production (Tg year^{-1})[c]	5486	4960	mean: 4900, range: 3800-6900[d]
O_x chemical loss (Tg year^{-1})	4983	4360	mean: 4600, range: 3300-6600[e]
Dry deposition (Tg year^{-1})	873	908	mean: 1000, range: 700-1500[f]
STE (Tg year^{-1})	370[g]	325[g]	mean: 500, range: 180-920[h]
Lifetime (days)	20.9	24.2	mean: 22.3, range:19.9-25.5[i]
Global OH (10^6 molecule cm^{-3}) [j]	1.16	1.25	mean±STD: 1.11±0.16, range: 0.74-1.33[k]
Methane chemical lifetime (years)	8.27		mean±STD: 9.7±1.5, range: 7.1-14.0[k]

[a] from Table 2 in Hu et al. (2017). The GEOS-Chem version is v10-01.

[b] from Figure 3 in Young et al. (2018), 49 models for 2000 condition.

[c] Budget is for the odd oxygen family, including O_3, NO_2, NO_y, several organic nitrates and bromine species) to account for the rapid cycling among O_x constituents. Ozone accounts for more than 95% of the total O_x.

[d] from Figure 3 in Young et al. (2018), 33 models for 2000 condition.

[e] from Figure 3 in Young et al. (2018), 32 models for 2000 condition.

[f] from Figure 3 in Young et al. (2018), 33 models for 2000 condition.

[g] estimated from the residual of mass balance between tropospheric chemical production, chemical loss, and deposition.

[h] from Figure 3 in Young et al. (2018), 34 models for 2000 condition.

[i] from Table 2 in Young et al. (2013), 6 models for 2000 condition.

[j] Global annual mean air-mass-weighted OH concentration in the troposphere

[k] from Table 1 in Naik et al. (2013), 16 models for year 2000. STD stands for standard deviation.

885

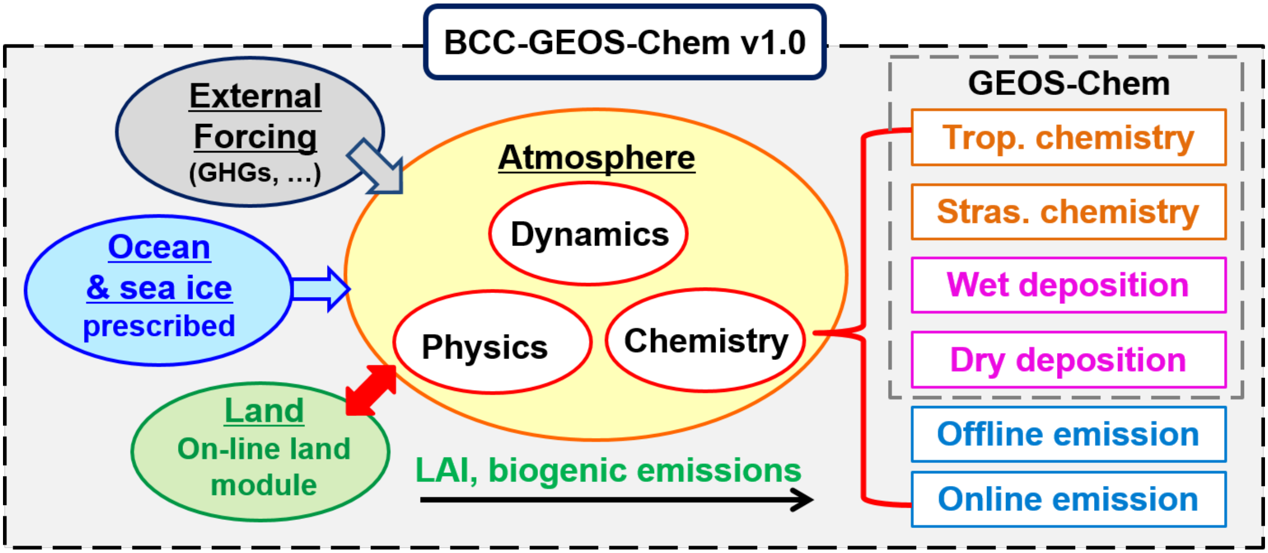

Figure 1. Schematic diagram of the BCC-GEOS-Chem v1.0 model framework.

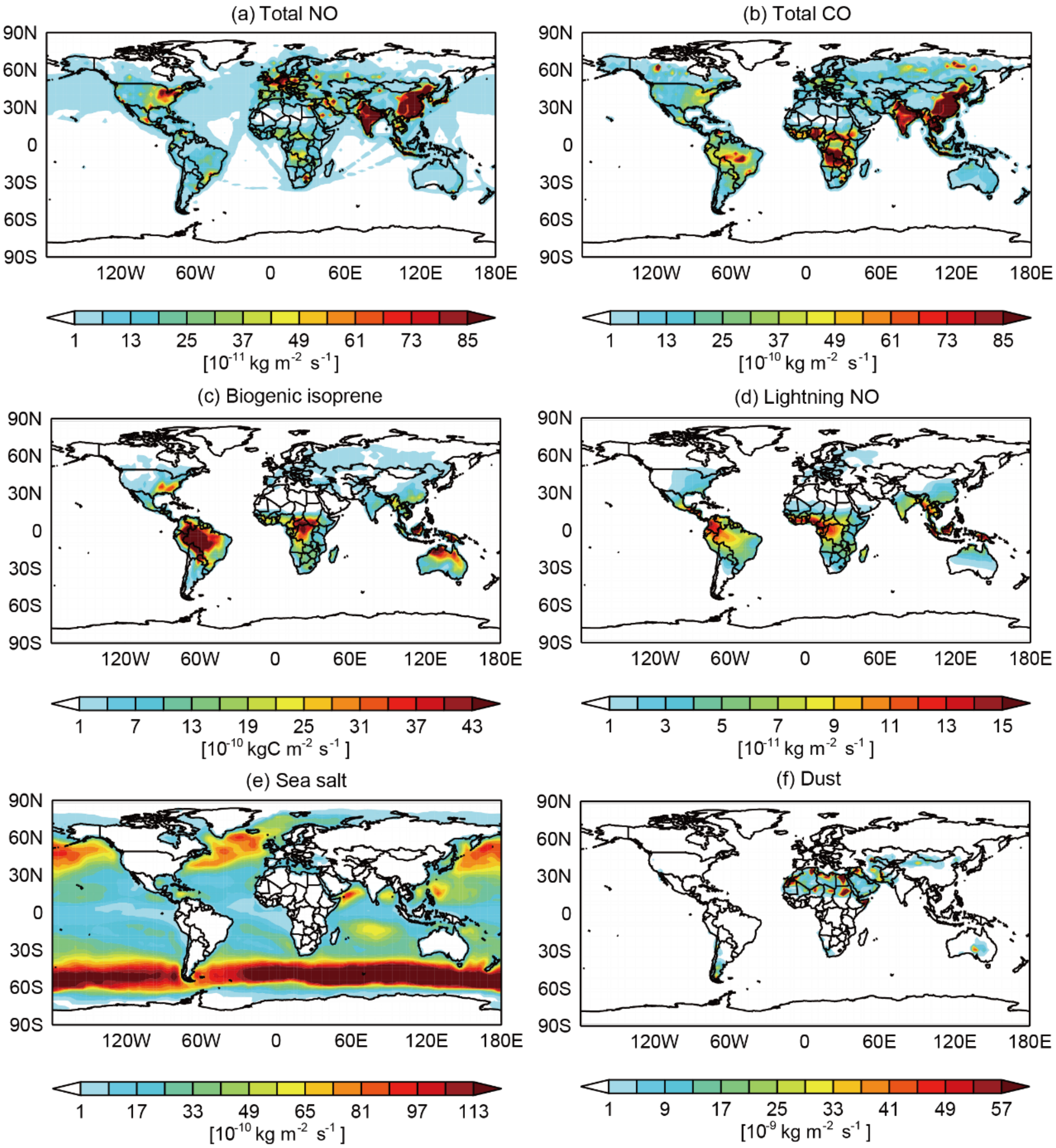

890 **Figure 2.** Spatial distributions of annual total emissions used in the study, (a) total NO emission (not including lightning emissions); (b) total CO emission; (c) biogenic isoprene emission; (d) lightning NO emission; (e) sea salt emission (dry mass); (f) mineral dust emissions.

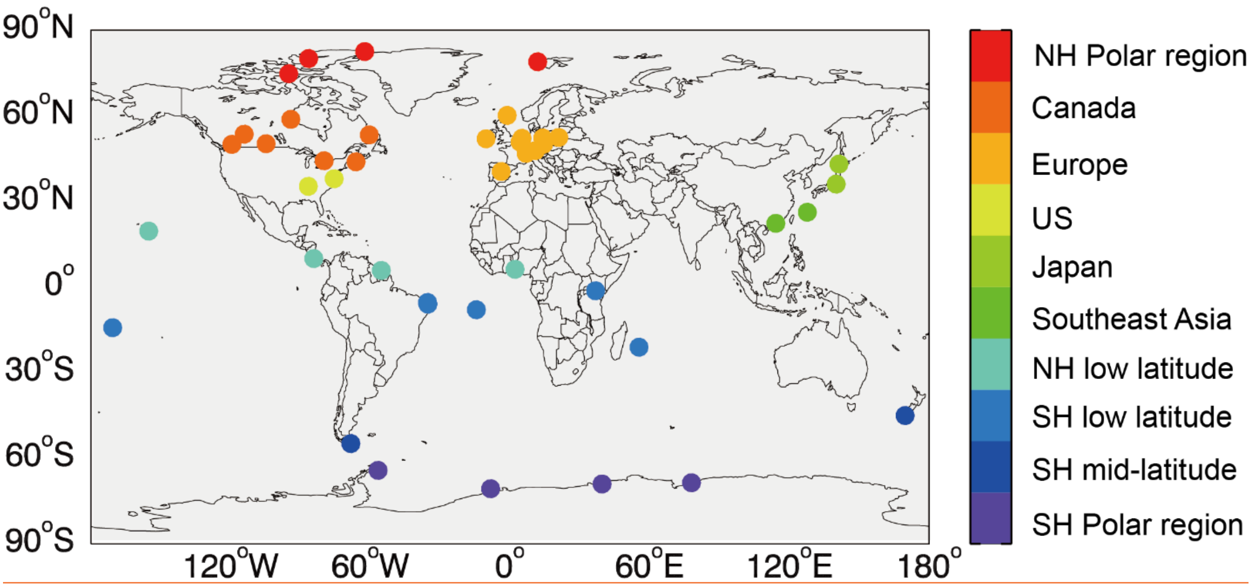

Figure 3. Locations of selected ozonesonde observations in 2012-2014 used in this study categorized by ten~~nine~~ regions.

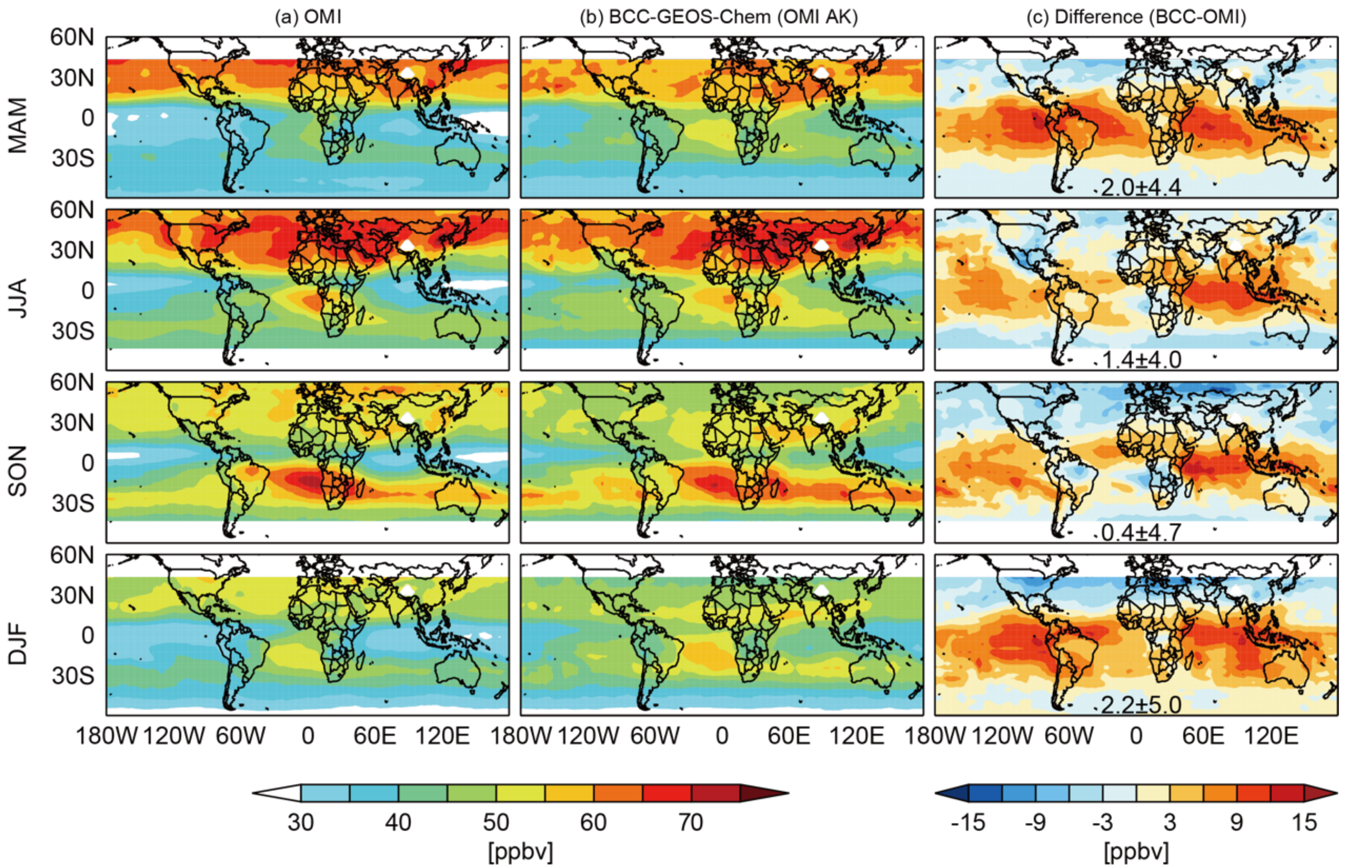

Figure 4. Spatial and seasonal distributions of tropospheric ozone at 700-400 hPa from (a) OMI satellite observations; (b) BCC-GEOS-Chem v1.0 model results (with OMI averaging kernels applied), and (c) differences between the two (model results minus observations) with the seasonal mean differences (±standard deviations) shown inset. Values are 3-year averages for 2012-2014.

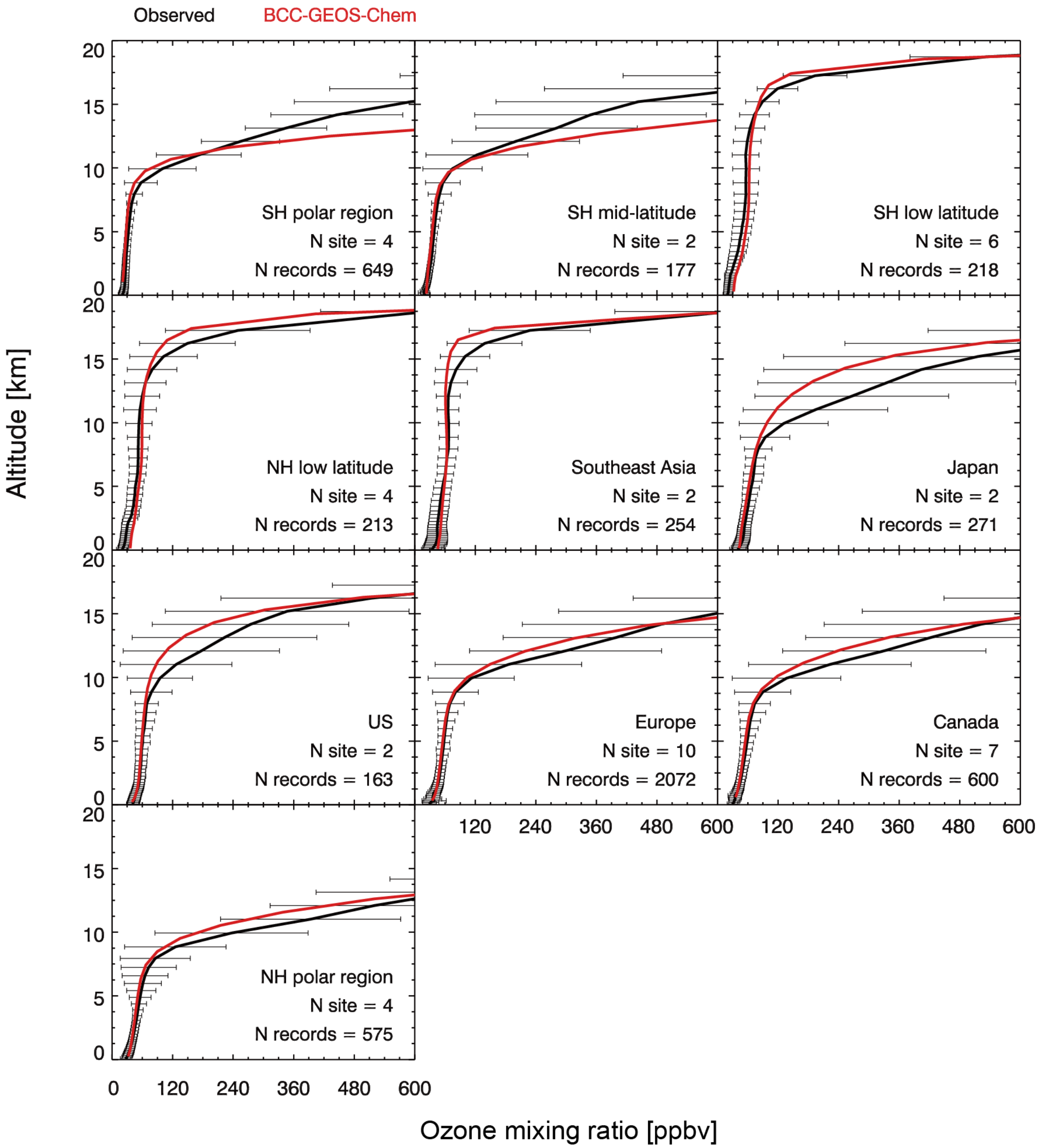

Figure 5. Comparisons of BCC-GEOS-Chem v1.0 simulated annual mean ozone vertical profiles to ozonesonde observations averaged over the ten~~nine~~ regions (Fig. 3) from south to north. Black horizontal bars are the standard deviations of observations. Numbers of available sites and records for each region in 2012-2014 are given inset.

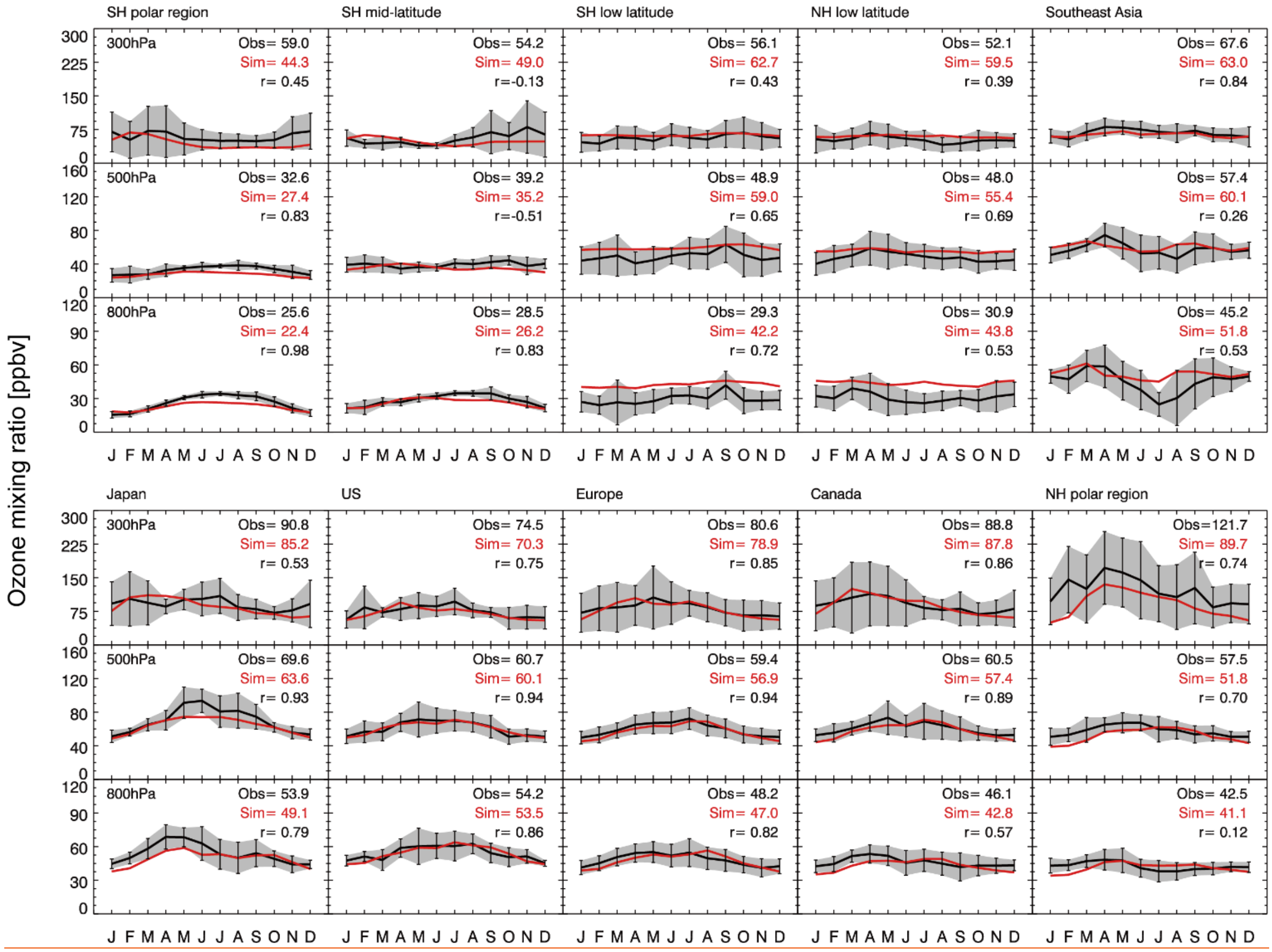

Figure 6. Seasonal variations of ozonesonde observed (black lines) and model simulated ozone (red lines) at three pressure levels (300 hPa, 500 hPa, and 800 hPa) averaged over the ten~~nine~~ regions (Fig.3). Vertical black bars and grey shadings are the standard deviations of observations. The annual means of observed and simulated ozone concentrations and their correlation coefficients are shown inset. Values are 3-year averages for 2012-2014.

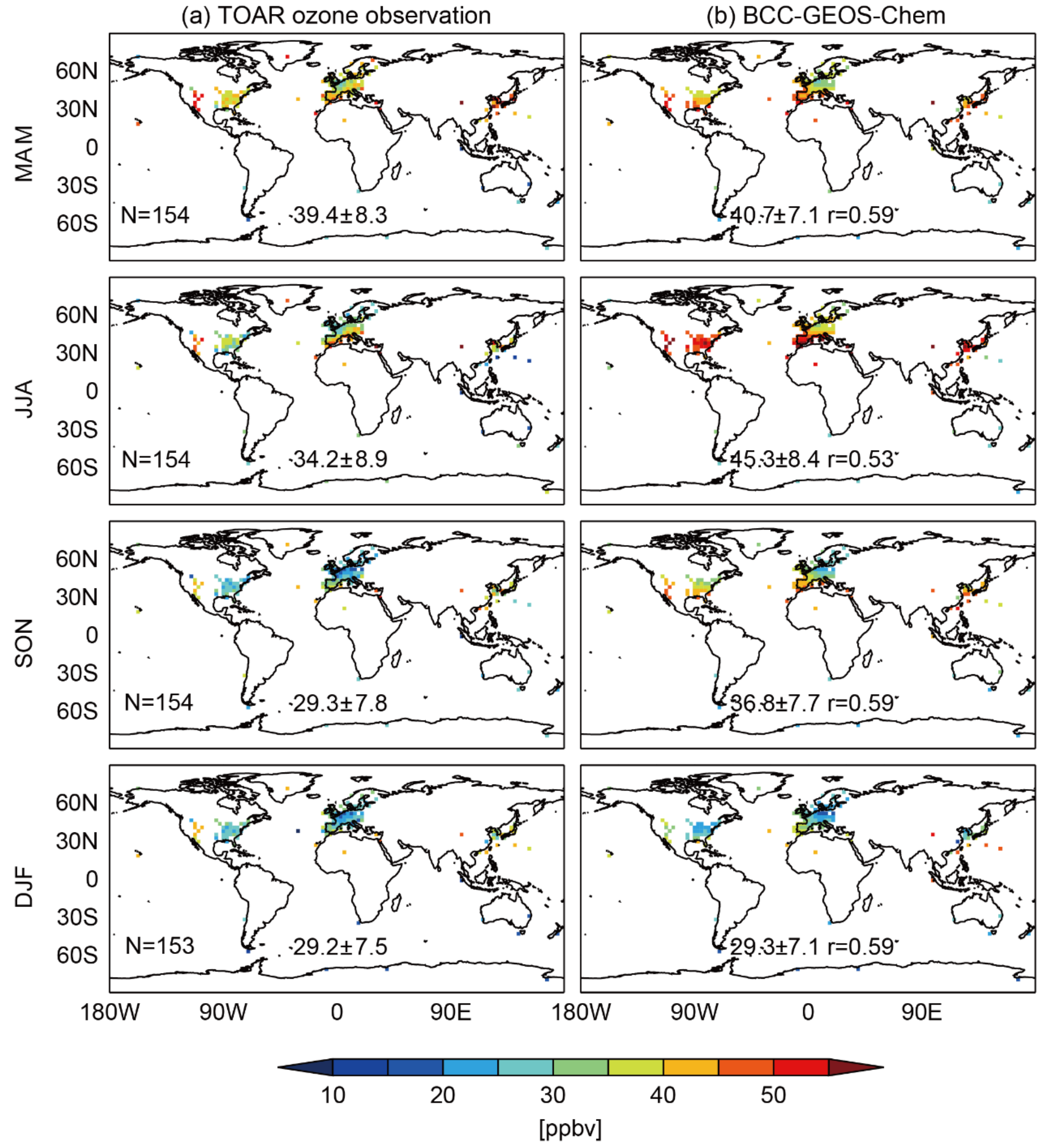

Figure 7. Spatial and seasonal distributions of observed and simulated surface ozone mixing ratios ~~(contours)~~ over 2012-2014. The model results (right panels) are compared to observations at rural/remote sites ~~(circles)~~ from the TOAR dataset (left panels). Observations are averaged to the same model grid. Seasonal mean values for observations and model results ~~(sampled at corresponding TOAR data sites)~~, their spatial correlation coefficients (*r*), and the number of co-sampled grids (N) are shown inset.

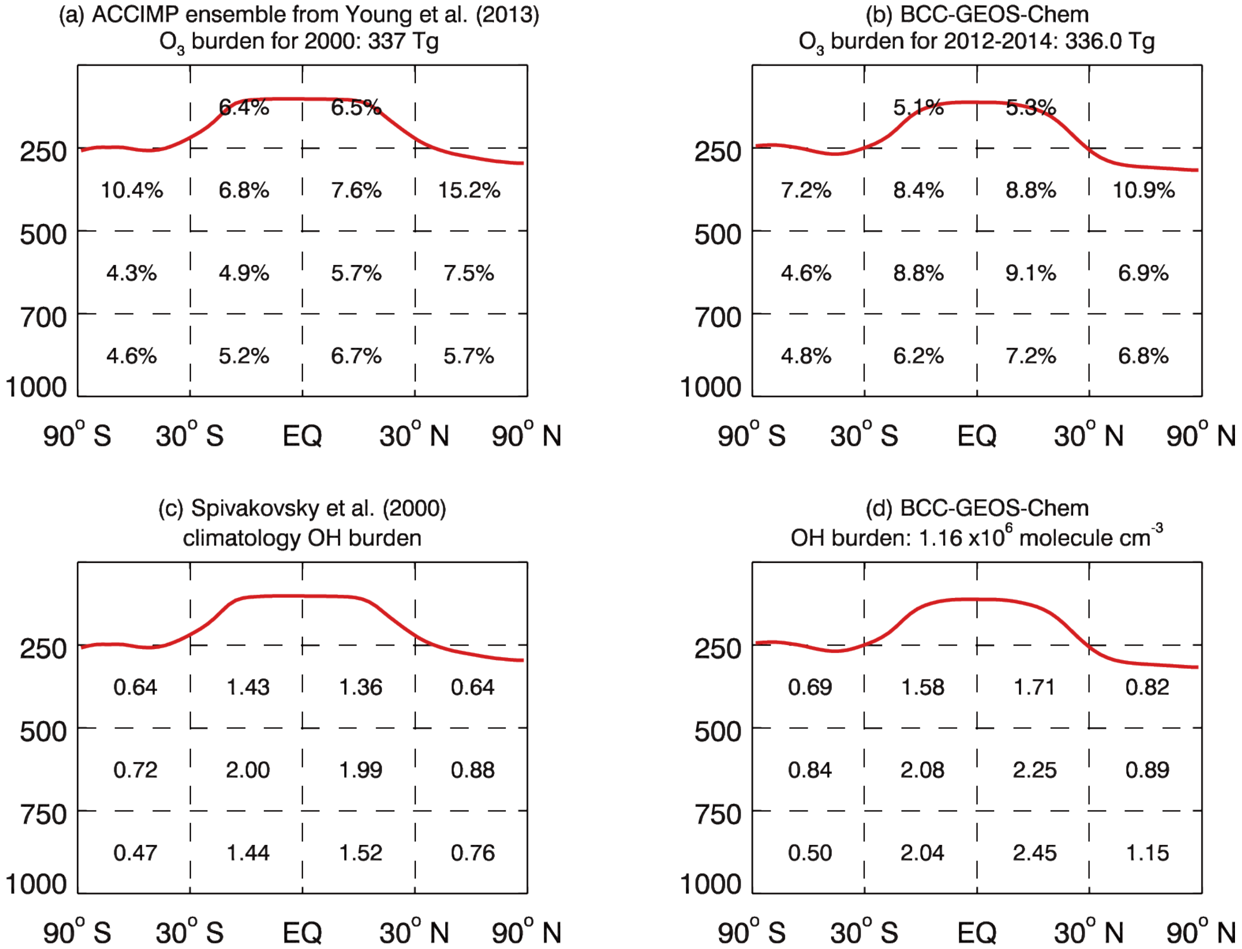

Figure 8. Zonal and vertical distributions of the tropospheric ozone burden and OH concentrations. For comparison, panel (a) shows tropospheric ozone burden in the year 2000 from Young et al. (2013) based on 15 ACCMIP models, and panel (c) shows climatological tropospheric OH burden reported by Spivakovsky et al. (2000) and summarized by Emmons et al. (2010). Panel (b) and (d) show corresponding results from BCC-GEOS-Chem v1.0 averaged over 2012-2014. The red lines in (a) and (c) denote the tropopause derived from the National Centers for Environmental Prediction (NCEP) reanalysis, and these in (b) and (d) are from BCC-GEOS-Chem v1.0.

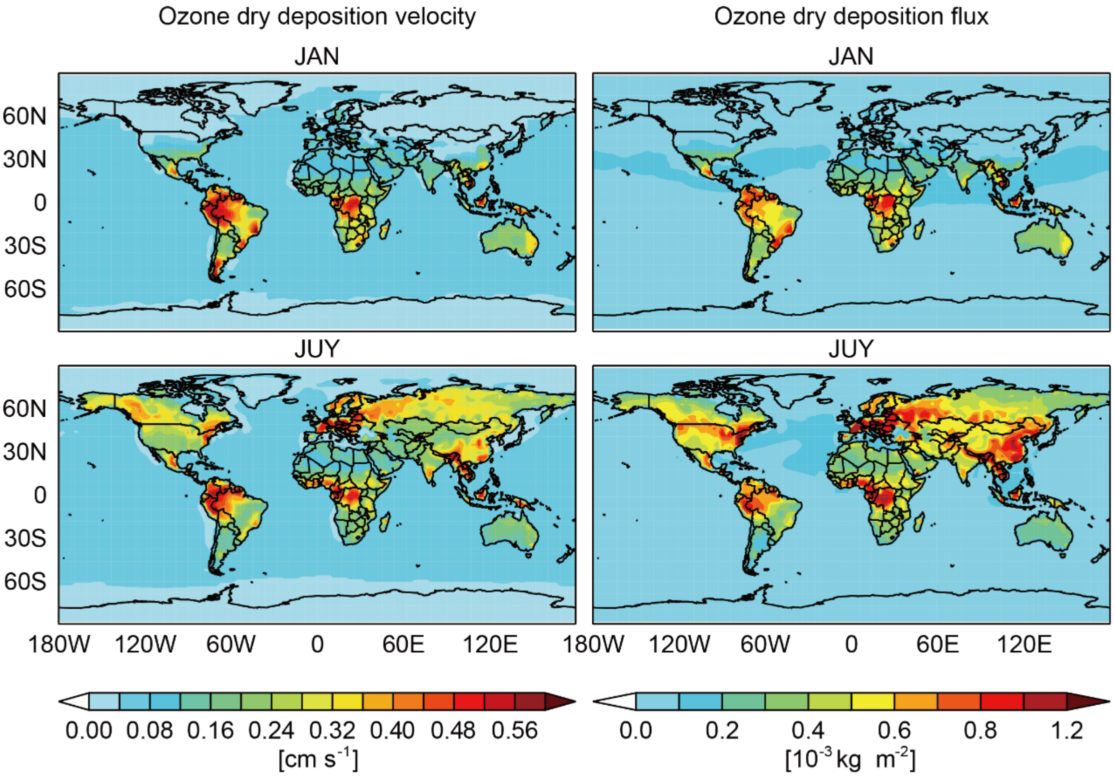

Figure 9. Monthly mean model diagnosed ozone deposition velocities (cm s^{-1}) and fluxes (kg m^{-2}) in January (top panels) and July (bottom panels).

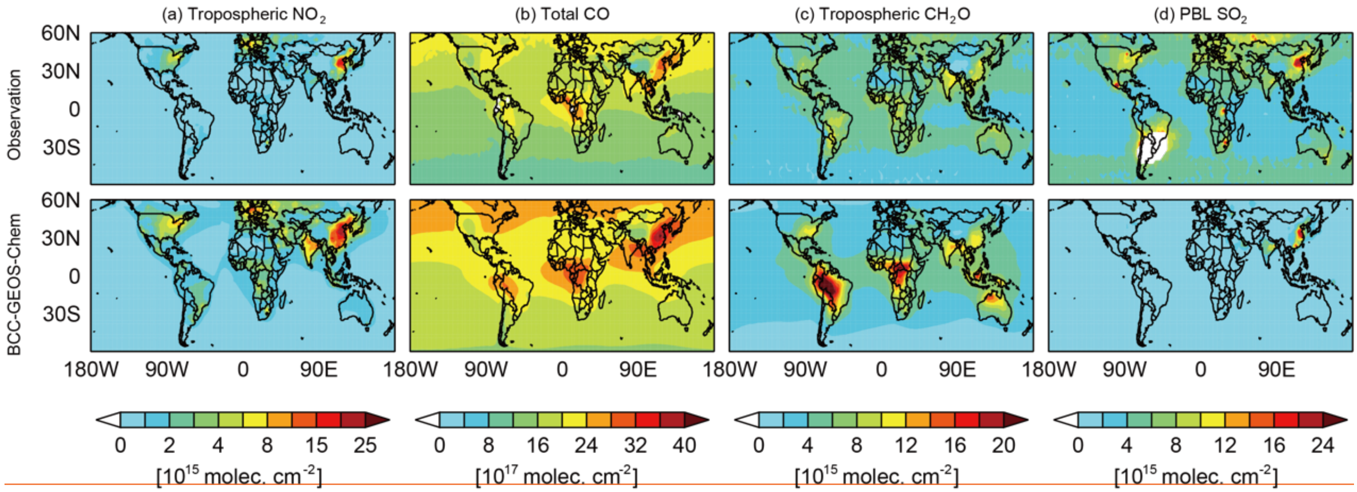

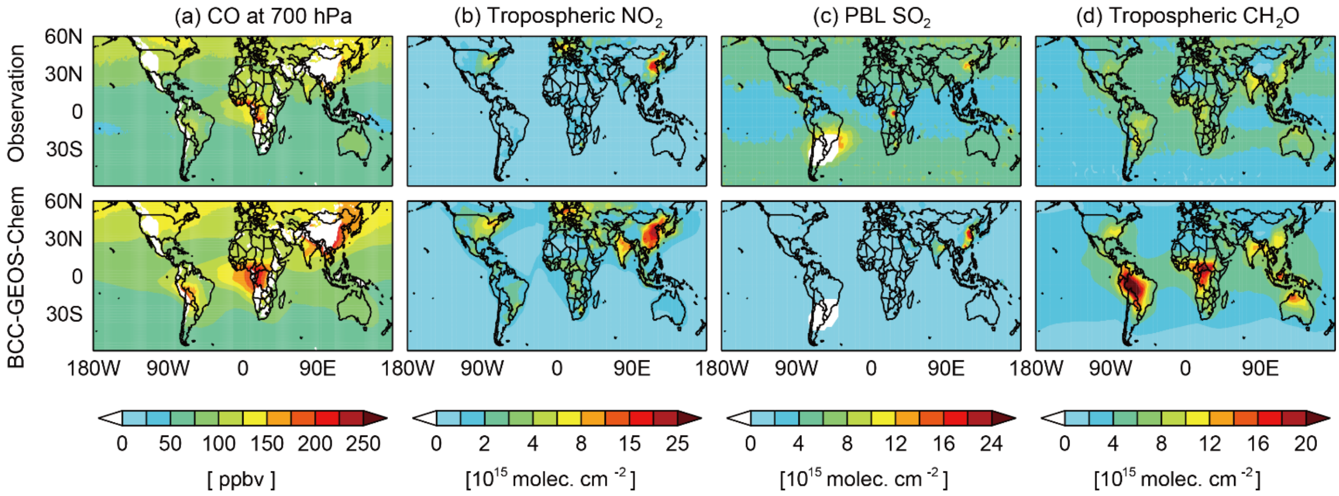

~~**Figure 10.** Spatial distributions of satellite observed (top panels) and model simulated (bottom panels) annual mean (a) tropospheric NO$_2$ column, (b) total CO column, (c) tropospheric CH$_2$O column, (d) SO$_2$ column in planetary boundary layer. Values are 3-year averages for 2012-2014.~~

Figure 10. Spatial distributions of satellite observed (top panels) and model simulated (bottom panels) annual mean (a) CO mixing ratio at 700 hPa, (b) tropospheric NO$_2$ column, (c) SO$_2$ column in planetary boundary layer, and (d) tropospheric CH$_2$O column,. Values are 3-year averages for 2012-2014.

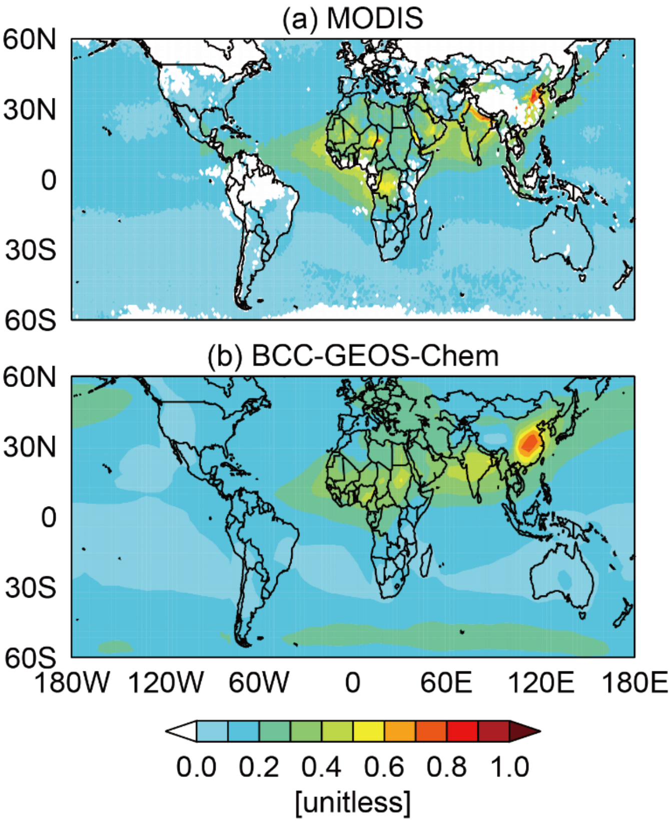

Figure 11. Spatial distributions of annual mean aerosol optical depth (AOD) at 550 nm from (a) MODIS satellite observations and (b) BCC-GEOS-Chem v1.0 averaged over 2012-2014.

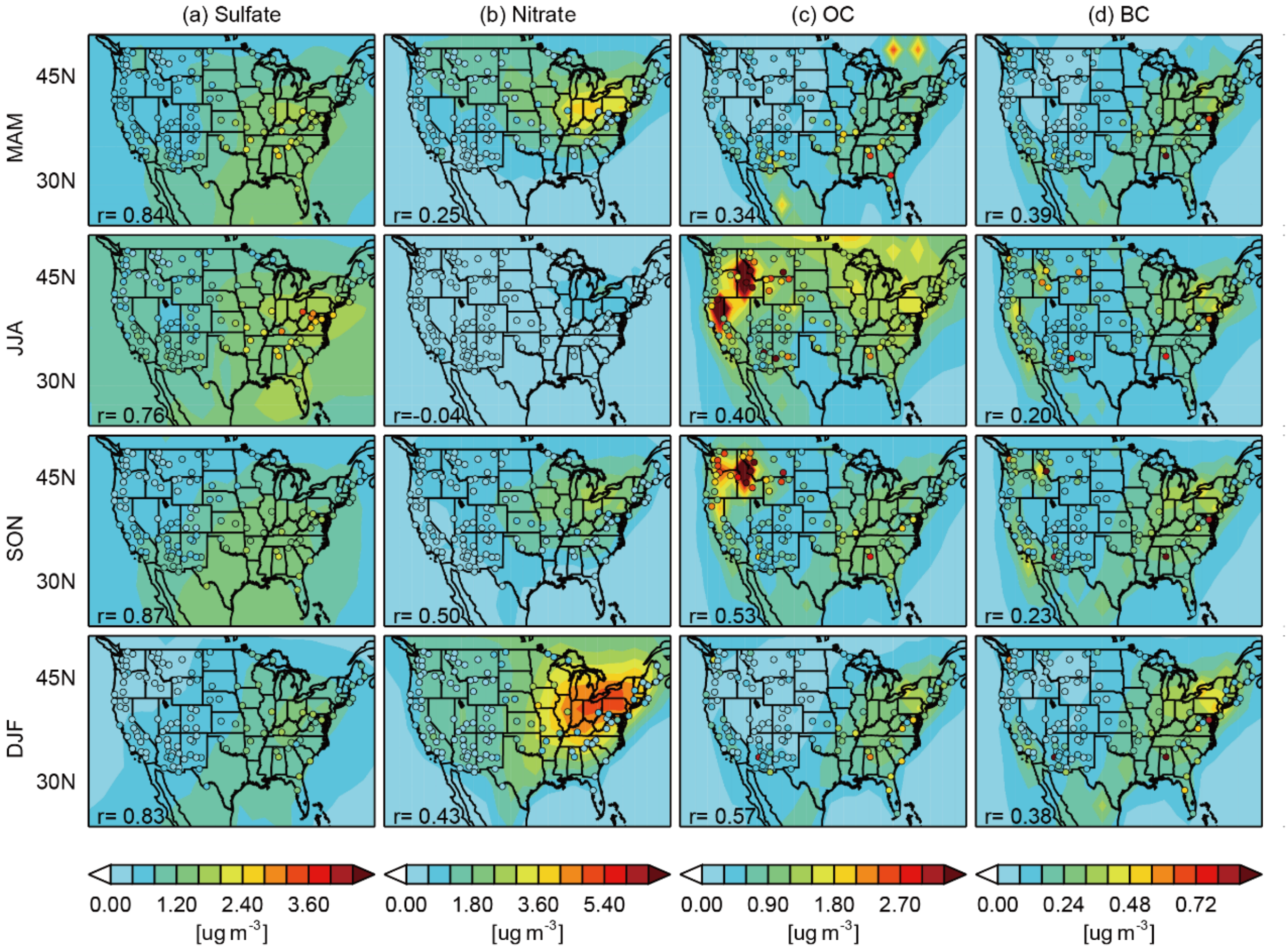

Figure 12. Spatial and seasonal distributions of simulated surface concentrations (contours) of (a) aerosol sulfate, (b) nitrate, 960 (c) organic carbon, and (d) black carbon compared with observations from the US IMPROVE network (circles) over 2012-2014. Correlation coefficients between observations and model results sampled at the site locations are shown inset.